EXPERIMENTAL INVESTIGATION OF THE RAYLEIGH-TAYLOR INSTABILITY

by

Roman Popil
B.Sc., University of Regina, 1977

A THESIS SUBMITTED IN PARTIAL FULFILLMENT
OF THE REQUIREMENTS FOR THE DEGREE OF
MASTER OF SCIENCE

in

THE FACULTY OF GRADUATE STUDIES

Department of Physics

We accept this thesis as conforming

to the required standard

THE UNIVERSITY OF BRITISH COLUMBIA

April, 1979

In presenting this thesis in partial fulfilment of the requirements for an advanced degree at the University of British Columbia, I agree that the Library shall make it freely available for reference and study. I further agree that permission for extensive copying of this thesis for scholarly purposes may be granted by the Head of my Department or by his representatives. It is understood that copying or publication of this thesis for financial gain shall not be allowed without my written permission.

Department of PHYSICS

The University of British Columbia
2075 Wesbrook Place
Vancouver, Canada
V6T 1W5

Date MARCH 22, 1979

ABSTRACT

The Rayleigh-Taylor instability of a water-air interface was investigated using electrical and photographic methods. An apparatus is described which accelerates a rectangular tank of water downwards and produces reproducible instabilities from a pure sinusoidal standing surface water wave of known phase and amplitude. The electrical measurements revealed that in addition to the bulk motion, films of water are produced on the walls of the water tank. The existence of these and other features of the instability are substantiated by photographs of the various instabilities that were produced. The electrical measurements led to a new scaling law for the phenomenon of climbing fluid films at accelerations greater than gravity. Several linear devices were also developed for measuring the amplitudes of surface water waves.

TABLE OF CONTENTS

LIST OF TABLES

LIST OF FIGURES

ACKNOWLEDGEMENT

This project was carried out under the auspices of Dr.F.L.Curzon whose keen interest in my stuggling endeavours and enthusiasm for science I found to be both encouraging and inspiring.

A.Cheuck's technical assistance with the electronics and innumerable other technicalities proved to be invaluable. M. Heinrich and G.Auchinleuck assisted with much of the machine shop work.

CHAPTER I

INTRODUCTION

Rayleigh-Taylor instabilities occur whenever there is an acceleration of the planar interface of two superimposed fluids such that the acceleration is directed from the less dense to the denser fluid. If the binary fluid system is left completely undisturbed a condition of an unstable equilibrium will exist. However, if the interface is initially perturbed prior to acceleration, the perturbation will grow exponentially with time, giving rise to the so called Rayleigh-Taylor instability.

This instability is a common occurrence in nature as in the formation of icicles, and the acceleration of stellar material on stellar surfaces. Rayleigh-Taylor instabilities are of current interest in plasma physics where the unstable surface is the plasma vacuum interface. They occur whenever the attempt is made to accelerate the plasma by a magnetic field as in a z-pinch or a tokomak. Perhaps the most common example can be taken to be the case of a glass of water turned upside down. Here, the acceleration is that due to gravity and is directed from the water to the air and thus the air-water interface is unstable. The water, instead of maintaining a nearly plane lower interface as it falls, will tend to be deformed into long spikes. It is the formation and rate of growth

of these spikes that has been the topic of several experimental and numerous theoretical investigations.

Shortly after the theoretical paper by G. I. Taylor (1950), the instability was investigated experimentally by D.J. Lewis (1950), who subjected a short column of water to a pressure difference in the air above and below the water. Emmons, Chang and Watson (1959) carried out a similar experiment in which a rectangular tank of water was accelerated downward by the force of stretched rubber tubing. At accelerations greater than that of gravity, the atmospheric pressure of the air takes the role of the lighter fluid being accelerated in the direction of the heavier one. Cole and Tankin (1972) and Ratafia (1973) have performed similar experiments where a rectangular tank of water was accelerated downward at accelerations several times greater than gravity.

The first order theory as originally formulated by G.I. Taylor follows easily from the conventional hydrodynamics. The free surface of the water is given by:

$$y=\eta(x,z,t)$$

where y is taken along the vertical axis, and x,z are rectangular coordinates in the horizontal plane. Differentiating this expression with respect to time t, yields the free surface boundary condition:

$$-\eta_t - u\eta_x + v = 0$$

where the subscripts denote partial derivatives and u, v are the horizontal and vertical components of the velocity. Bernoulli's law upon neglecting second order terms in the velocity gives an expression for the pressure:

$$p = p_o - (g + g_1)\rho y + \rho\Phi_t$$

where $(g + g_1)$ is the virtual acceleration seen by the interface, ρ is the density of the fluid and Φ is the velocity potential which satisfies Laplace's equation:

$$\nabla^2\Phi = 0$$

and whose gradient gives the components of the velocity:

$$\underline{v} = (u,v,w) = \nabla\Phi$$

The theory considers two superimposed fluids each with a pressure, density and velocity potential.

For the upper fluid (air), the velocity potential and pressure are :

$$\Phi_1 = A\exp\{-ky\}f(t)\cos\{kx\}$$

$$p_1 = p_o - (g + g_1)\rho_1 y + \rho_1(\Phi_1)_t$$

Similarly, for the lower fluid the corresponding quantities are:

$$\Phi_2 = -A\exp\{-ky\}f(t)\cos\{kx\}$$

$$p_2 = p_o - (g + g_1)\rho_2 y + \rho_2(\Phi_2)_t$$

where $k=2\pi/\lambda$ is the wavenumber, and λ is the wavelength of the periodic instability.

The form adopted for the velocity potentials is that for standing waves that satisfy the boundary conditions that the velocities be finite at $y = \pm\infty$, that they be equal at the interface $y = 0$ and that $\underline{v} \cdot \underline{n} = 0$ on the tank walls where $\underline{n}$ is the normal vector to a wall.

The nonlinear term $\eta_x u$ in the free surface condition is neglected yielding

$$\eta_t = v = (\Phi_i)_y$$

$$= -kAf(t)\cos\{kx\}$$

which upon integration becomes:

$$\eta = -kA(\int_{t_o}^{t} f(t)dt)\cos\{kx\}$$

At the interface, the pressures p_1 and p_2 are equal. This condition, when used with the expression for η, leads to:

$$-(g + g_1)(\rho_2 - \rho_1)kf(t)$$

$$-(\rho_2 + \rho_1)f''(t) = 0$$

The theory is considerably simpler at this point, if the requirement is made that at $t = 0$ and $y = 0$ the fluid velocity is zero. This is satisfied if the time dependence is

$$f(t) = \sinh\{nt\}$$

where n is the growth rate of the instability.

The condition for equal pressures now gives an explicit expression for the growth rate:

$$n^2 = \frac{-(g + g_1)(\rho_2 - \rho_1)k}{(\rho_2 + \rho_1)}$$

Hence, the interface as a function of time is given by the expression:

$$\eta = kAn^{-1}\cosh\{nt\}\cos\{kx\}$$

Therefore, if the quantity $(g + g_1) < 0$ then the growth rate n is positive and the disturbance grows exponentially.

Bellmann and Peninigton (1954) considered the effects of surface tension and viscosity. For an air-water interface, the effects of viscosity are negligible. Surface tension T, is introduced through the equal pressures condition:

$$p_2 - p_1 + T\eta_{xx} = 0$$

The resulting expression for the growth rate becomes:

$$n^2 = \frac{-(g + g_1)(\rho_2 - \rho_1)k}{(\rho_1 + \rho_2)} - \frac{Tk^3}{(\rho_1 + \rho_2)}$$

If $n^2 > 0$ the surface is unstable. It is evident from the above expression that the surface tension stabilizes modes with a wavelength:

$$\lambda < 2\pi\left(\frac{T}{-(g + g_1)(\rho_2 - \rho_1)}\right)^{\frac{1}{2}}$$

since for such wavelengths $n^2 < 0$.

Thus for initial disturbances whose wavelengths are smaller than the above, there is no instability. This explains why small droplets cling to the underside of a horizontal surface such as a ceiling. For water, under the action of gravity, the critical wavelength is 1.73 cm so that droplets of a larger radius will tend to drip while smaller ones will hang.

The first order theory as formulated by G. I. Taylor does not account for the later stages of the instability where the crests develop into long spikes and the troughs into rounded bubbles (Figure 1). Lewis's investigations led to the conclusion that the first order theory is valid only until the amplitude of the spikes is about 0.4λ.

By assuming that the surface disturbance and velocity potentials can be expanded in a power series, Emmons et al. determined how the later stages of the instability evolve. The harmonic content of the distorted growing disturbance is given by the Fourier series:

$$\eta = \sum_{m=1}^{\infty} A_m(t)\cos\{mx\}$$

The original purpose of this experiment was to follow the development of the Fourier spectrum of the initial perturbation with time. To this purpose, a capacitative Fourier analyzing technique as developed by Curzon and Langille (1972) was used. This method

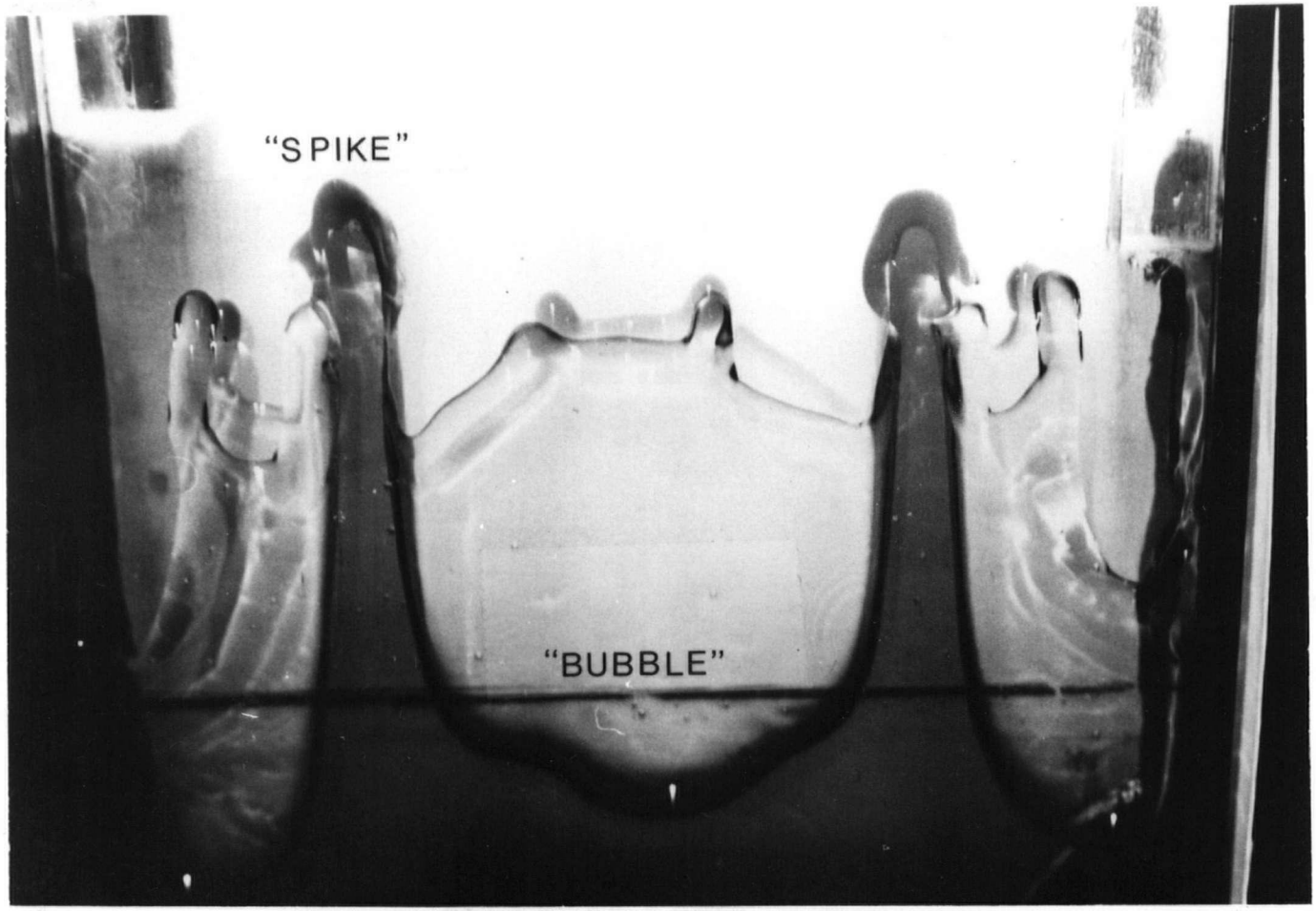

Figure 1. Photograph of a Rayleigh-Taylor instability arising from the fourth harmonic standing wave. The "spike" and "bubble" are indicated.

analyzes each harmonic mode separately i.e., it essentially measures $A_m(t)$ for selected m. The assumption is made that the variation in the area of the plates and depth of the water is in the x direction only so that the capacitance is calculated as an integral over the x variable. For the system used in the experiments, the water, whose conductivity is increased by adding some acid forms one plate of a parallel plate capacitor. The other plate, separated from the first by a thin polyethylene sheet forms one wall of the water tank. It consists of a number of equally spaced vertical strips whose width W(x) is a function of x and is given by:

$$W(x) = W_o(1 - \cos\{q\pi x/L\}) \qquad (1)$$

where W_o = constant, q is an integer equal to the mode number that is to be analyzed and L is the length of the tank.

Hence, for a small increment dx, the capacitance is given by:

$$dC = \frac{\kappa\varepsilon_o}{d}(NW(x)y(x))dx \qquad (2)$$

where κ is the dielectric constant, ε_o the permittivity of free space, d is the thickness of the dielectric sheet and N is the number of strips per unit length. The elevation of the water surface can generally be expressed by a Fourier series expansion:

$$y = y_o + \sum_{r=0}^{\infty} \xi_r \cos\{r\pi x/L\} f_r(t)$$

The y_o term is the mean level of the fluid which is assumed to be constant and independent of the time if the motion is purely two dimensional. ξ_r is the amplitude of the rth harmonic of the surface disturbance and $f_r(t)$ is the time dependence. Therefore, the increment in capacitance is:

$$dC = (y_o + \sum_{r=0}^{\infty} \xi_r \cos\{r\pi x/L\} f_r(t))$$

$$X \ (1 - \cos\{q\pi x/L\})dx$$

The integration over x leads to

$$C = A(y_o L - \int_0^L \sum_{r=1}^{\infty} \xi_r \cos\{q\pi x/L\}$$

$$x \cos\{r\pi x/L\} f_r(t) dx)$$

$$= A(y_o L - \xi_q \frac{L}{2} f_q(t))$$

where the orthogonality of the cosines is used in the last step and A is a constant. Thus the time dependence of the capacitance is proportional to the time dependence of the qth harmonic of the surface disturbance.

The sensitivity of the technique is determined by noting that the change in capacitance ΔC due to an overall increase of water depth of amount h is twice the change in capacitance due to a qth harmonic wave of the same amplitude:

$$\frac{\Delta C \text{ water depth}}{\Delta C \text{ harmonic wave}} =$$

$$\frac{\frac{\kappa\varepsilon_o N}{d}\int_0^L W_o(1 - \cos\{q\pi x/L\})h\,dx}{\frac{\kappa\varepsilon_o N}{d}\int_0^L W_o(1 - \cos\{q\pi x/L\}h\cos\{q\pi x/L\}\,dx} = 2$$

A resistance Fourier analyzing technique works along the same principles. In this method, two Fourier analyzing plates are placed along two sides of the water tank with the conducting water between them. Then the resistance is given by:

$$R = \frac{\rho l}{A}$$

where ρ is the resistivity, l the distance between the two plates and A is the area given by the product of the strip width and depth of the water as in equation (2).

In the capacitance measuring technique, the capacitance is measured by the output signal of an impedance bridge while in the resistance method the voltage across the tank is observed.

Details of the equipment required to produce and measure R-T instabilities are now presented in the following chapter.

CHAPTER II

EXPERIMENTAL APPARATUS

A. Tank acceleration system

The Plexiglas tank containing the water-air interface is accelerated downward by the force supplied by a driven piston which is supplied with compressed air from a large reservoir and air tank. The reservoir ensures that the change in pressure supplied to the piston is in the order of only a few percent during the length of its run. The piston's cylinder is as long as the tank's length of travel (450 mm) so that there is a nearly constant force supplied to the tank throughout its motion.

By using a laser beam and a phototransistor to determine times of travel under various applied air pressures, the acceleration was found to increase linearly with the air pressure. For the cylinder of inner bore of 25.4 mm the increment was found to be 0.1g/p.s.i., g being the acceleration in free fall. The maximum pressure normally apllied was 25 p.s.i. so that the maximum virtual acceleration (i.e., the acceleration of the tank minus the acceleration of free fall) was 2.5g.

Since any initial surface perturbation will grow exponentially under such an apllied acceleration, care must be taken to release the tank at t = 0 in such a fashion that the water is not appreciably disturbed. To this end, a tank release mechanism was devised by

cutting away part of the wall of a brass tube. The remaining portion subtends an angle of 90 degrees at the axis and supports a horizontal brass rod which fastens onto the base of the water tank. The releasing brass tube is in turn mounted onto the aluminum frame of the tank accelerator. To release the tank, the release tube is rotated by a solenoid relay , so that the brass rod is no longer supported by the tube.The tank slides on two vertical steel rails at either side before coming into contact with the shock absorbers at the end of the shaft, (Figures 2 and 3). The shock absorbers are spring loaded pistons which are connected together by an exhaust air valve which is adjusted to achieve optimum stopping conditions.

B. Tank and Analyzing Plates

The water tank's sides and base are constructed from ¼ inch and 3/4 inch Plexiglas sheet respectively. The length, width and height are 188 x 107 x 200 mm. When used in capacitance measurements the water in contact with the largest walls of the rectangular tank (Figure 4) forms one plate of a capacitor and the second plate is adjacent to one of the 188 x 107 mm sides. A rubber O - ring is fitted along the perimeter of this to make the tank leakproof. The capacitor plate is insulated from the water by a thin polyethylene sheet of thickness

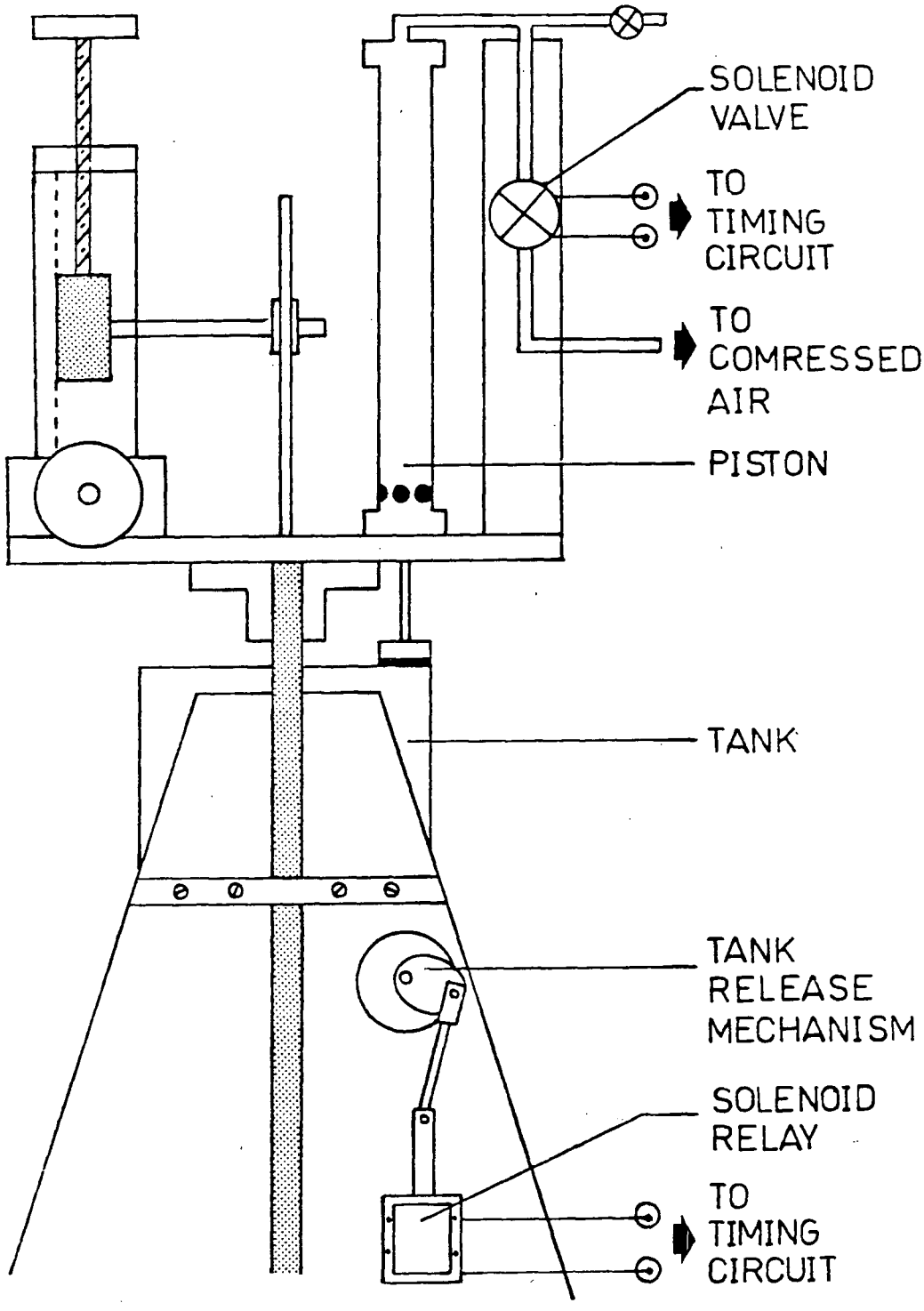

Figure 2. Side view of the tank accelerator.

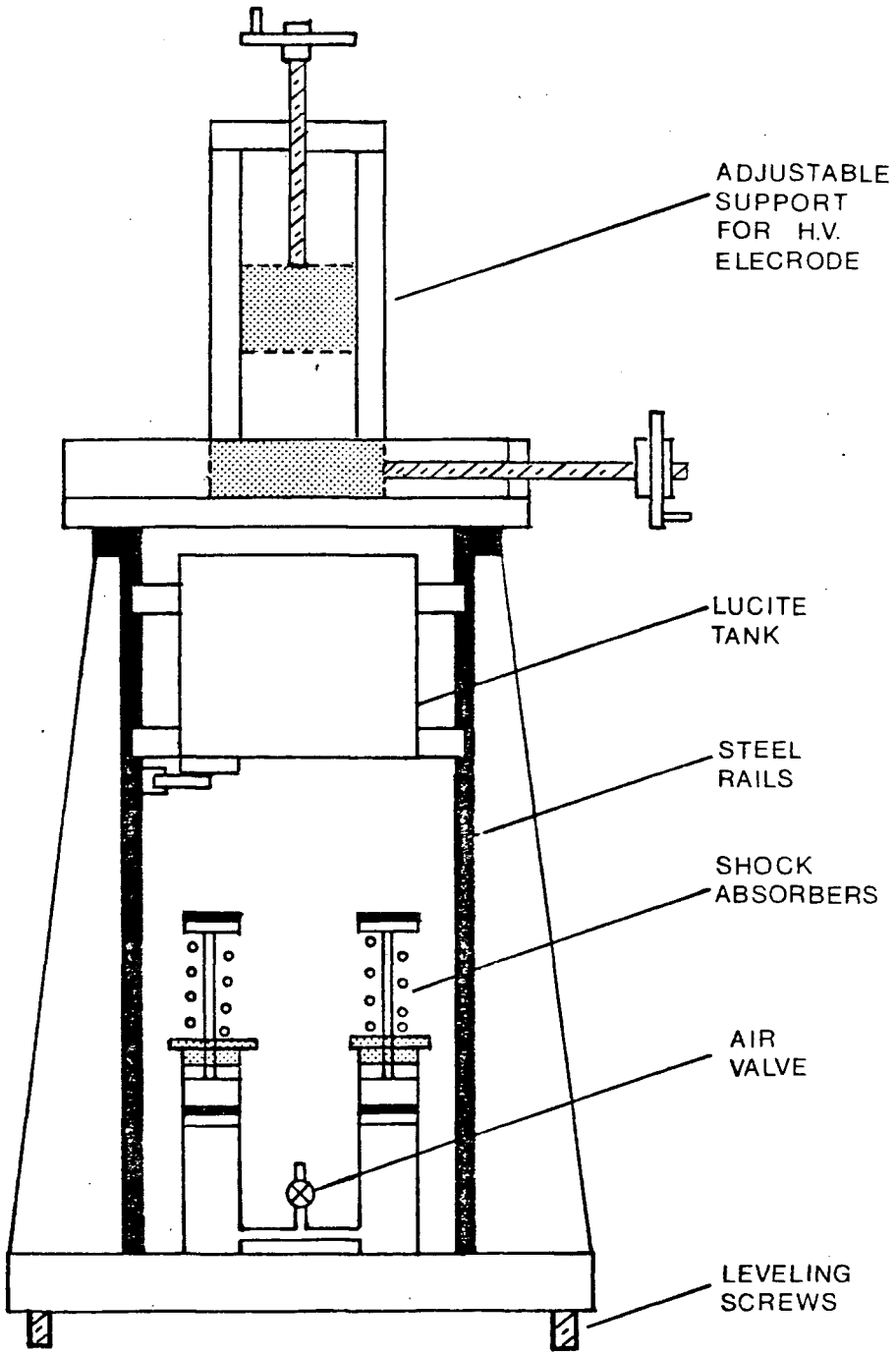

Figure 3. Front view of the tank accelerator.

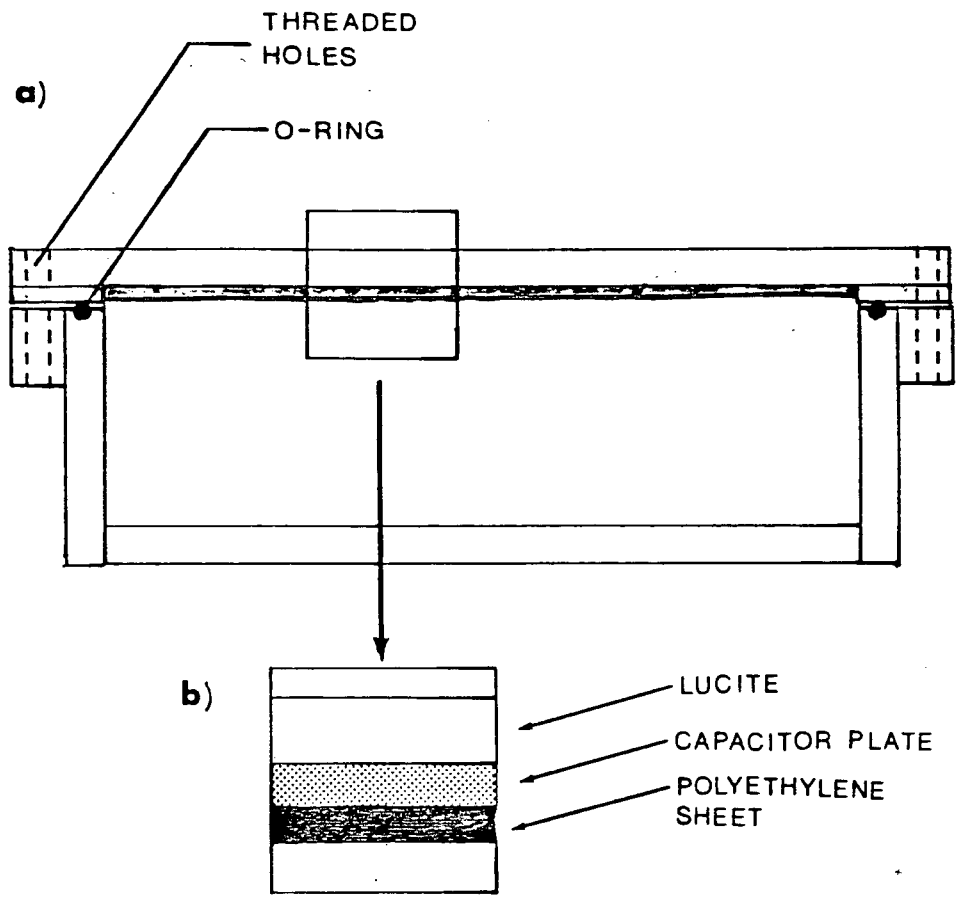

Figure 4a) Horizontal section of the water tank.
b) Detail of one side containing the capacitor and dielectric sheet.

0.077 mm placed between the O - ring and the capacitor plate. In earlier experiments, varnish and epoxy resin were used for the insulator but these materials proved to be ineffective because of small pinholes which leaked current. To analyze the water waves, the capacitor plate consists of vertical strips of copper whose width varies sinusoidally as given by equation (1) in the Introduction. In the experiments, W_o was chosen to be 0.5 cm and the mode number q was varied from 1 to 5 (Figure 5). The Fourier analyzing plates are made from printed circuit board using the standard photographic etching technique.

C. Wave Excitation

Standing pure modes are generated on the water surface by applying an alternating high voltage of the form:

$$V = V_o(\{1 - \cos(\omega t)\}/2)^{\frac{1}{2}}$$

where V_o is constant equal to 4.7KV, and ω is the resonant frequency of the desired surface wave in the water. The resonant frequency is determined to an excellent approximation by the dispersion relation for standing water waves which may be taken to be :

$$\omega^2 = gk\tanh(kh)$$

where h is the depth of the fluid in the tank.

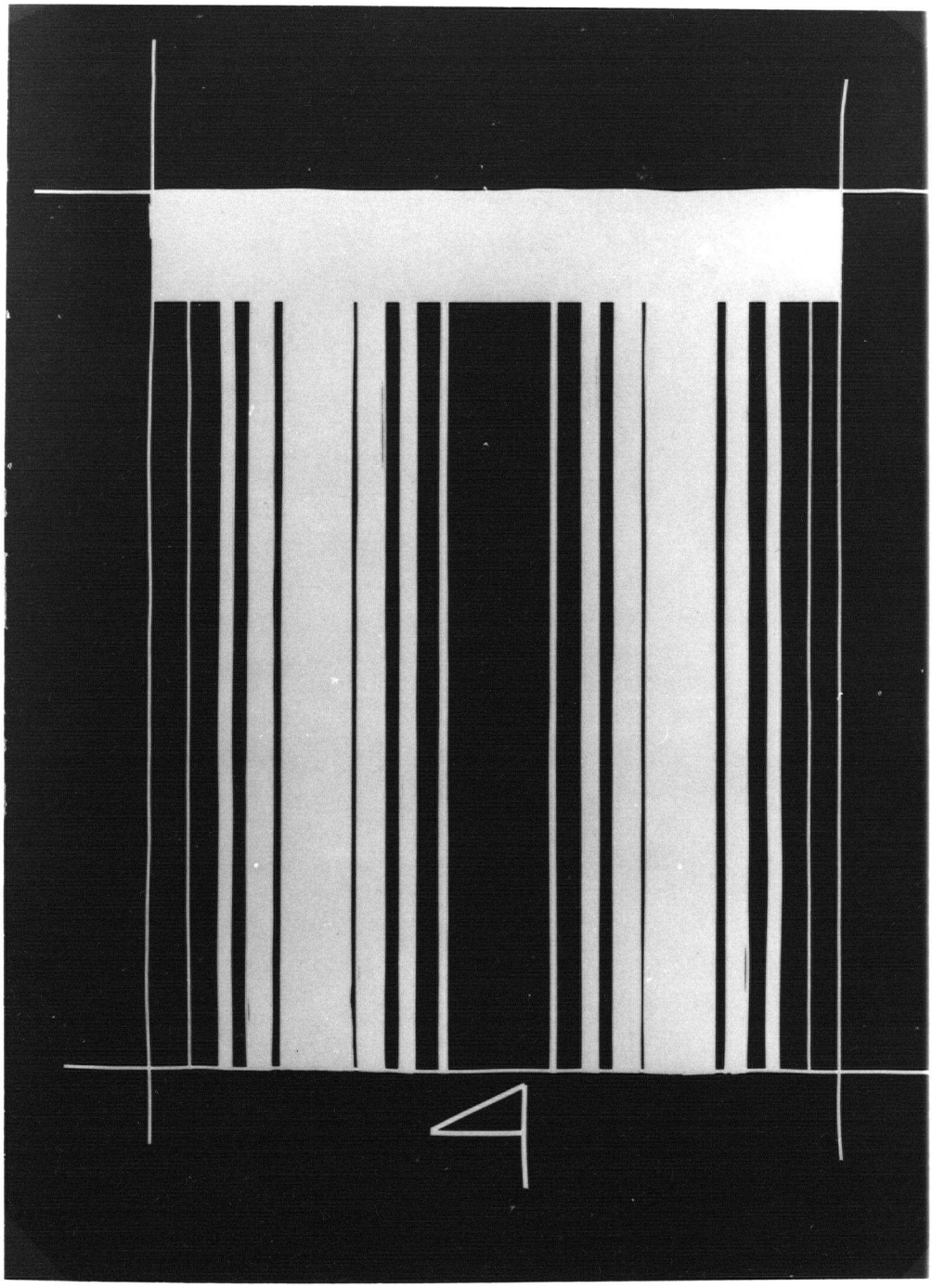

Figure 5. The fourth harmonic (q=4) Fourier analyzing plate.

To excite the waves using the periodic high voltage, horizontal electrodes are positiones over the water surface. The dimensions and positions of the electrodes varied with the mode excited and are summarized in the table below:

TABLE I : WAVE EXCITATION ELECTRODES

MODE NUMBER	NUMBER OF ELECTRODES	LENGTH	POSITION*
1	1	L/2	L/2
2	1	L/2	L/4
4	2†	L/4	L/8
8	4†	L/8	L/16

* Distance from right end of tank to the edge of the first electrode.

† Electrode spacing = electrode length.

The width of the electrodes are about equal to the width of the particular tank used. In all cases, the electrodes were polished and the edges rounded to minimize sparking to the grounded water. To adjust the distance between the electrode and the water surface, the former was supported by a vertical threaded rod (Figure 2). The plane of the electrode could be adjusted by leveling screws (Figure 6).

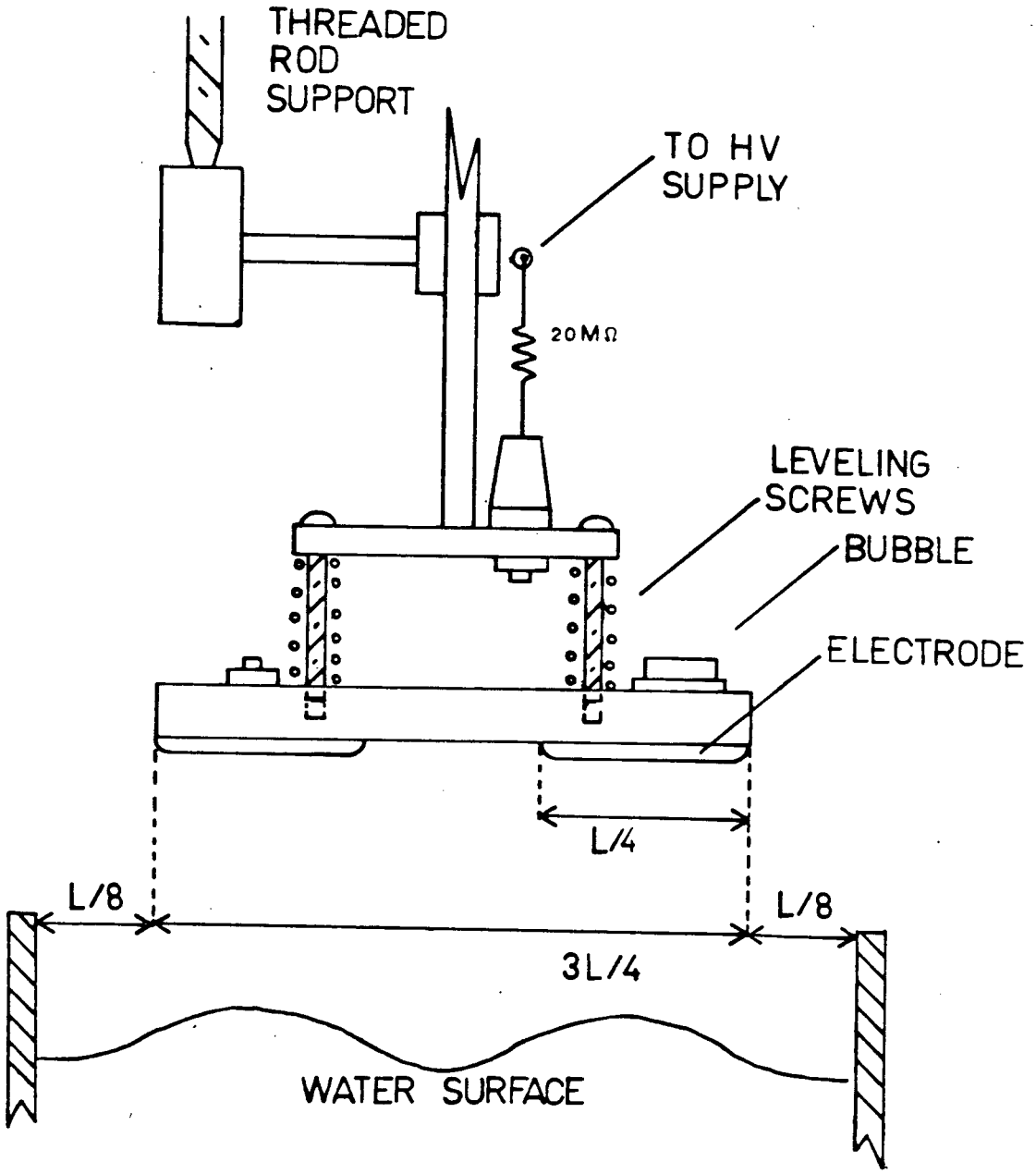

Figure 6. The electrode used to generate the fourth harmonic standing surface wave.

The alternating high voltage waveform is produced by a programmable digital waveform generator the details of which are given in the Appendix. The waveform generator stores one half of the desired waveform which is entered manually on two standard 4 x 16 RAM memory I.C. chips. An up/down counter together with a logic circuit that periodically reverses the direction of the count sweeps the 16 words of the memory. The output of the memory is then converted to an analog signal which is amplified by an operational amplifier (Kepco) to produce a periodic high voltage at the electrodes above the water. A 20MΩ resistor is used between the electrodes and the amplifier for protection of the circuitry in the event of sparking.

D.The Electrical System

The displacement η of the water-air interface excited by the electrostatic field is of the form:

$$\eta = A\cos(\omega t + \phi)\cos(kx)$$

where ϕ is the phase of the wave. If at the time of release of the tank ($t = 0$) the phase is 0 or π so that η is at a maximum, then the subsequent unstable wave grows at the rate given by the first order theory

described in the Introduction. The release of the tank at this fixed phase has the particular advantage that the resulting instabilities are reproducible.

To release the tank at the right instant of time, a comparator timing circuit is used. The electrcal system is shown in Figure 7. The timing circuit triggers on the output voltage of the digital waveform generator when its output voltage matches that preset on the comparator. A time delay is then adjusted so that the tank release pulse operates at the instant the standing wave is at maximum amplitude. This done by having two Fourier analyzing plates immersed in the water at opposite sides of the tank. The plates are connected to a series resistance of 2KΩ and a 50 V d.c. power supply. The voltage across the 200 ohms of acidified water is observed on a storage oscilloscope. Since the resistance varies inversely with the cross sectional area of water between the plates, an increase of area due to wave motion results in a decrease in voltage. Thus, the delay on the timing circuit was adjusted so that whenever the tank release pulse fired, the minimum of the sinusoidal signal was displayed at $t = 0$.

The comparator timing circuit produces two simultaneous pulses, one of which is used to release the tank and the other to open the solenoid valve and

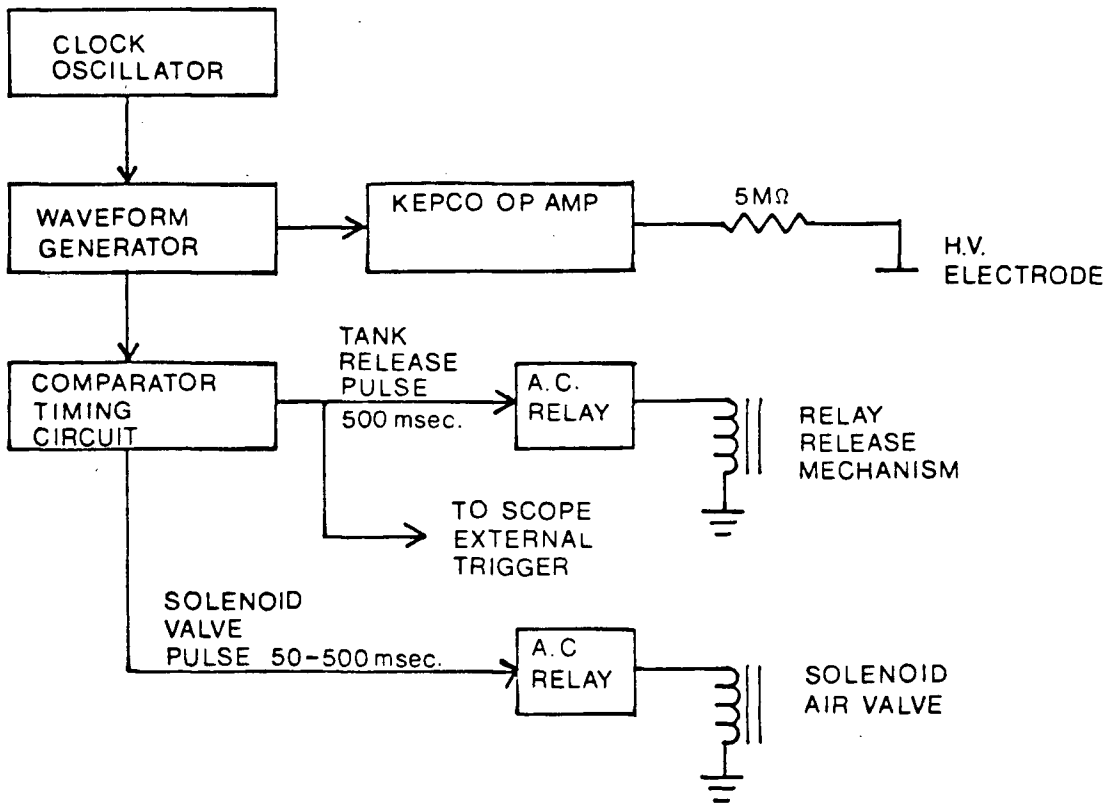

Figure 7. Block diagram of the electrical system.

and supply the piston with compressed air. The latter pulse has its width adjustable in the range 50 - 500 msec so that the solenoid valve will be open for the entire duration of the motion of the tank. The digital pulses are used to switch the mains voltage to the solenoids by means of solid state relay units.

E. The I.C. Capacitance Measuring Circuit

Besides using an impedance bridge to measure changes in capacitance with time, a simple capacitance measuring circuit was also developed and utilized (Popil and Curzon 1979). The circuit (Figure 8) essentially consists of one integrated circuit chip that determines the unknown capacitance by means of a frequency to voltage conversion. The best sensitivity of the circuit was found to be at an input frequency of 3KHz. For good linearity, C_1 was set at 1 μF and R_1 at 500 KΩ (10 turn Helipot). R_1 was adjusted so that the output was 4 volts when the tank was filled to depth of 9 cm from the bottom. Linearity is achieved only if the conductivity of the water is increased by adding 1 ml of 18 molar sulfuric acid to 2 liters of water (Figure 9). Under these conditions, the sensitivity of the circuit is 38 mV/mm of water. The calibration was done simply by noting the output voltage of the circuit as a function of the water depth.

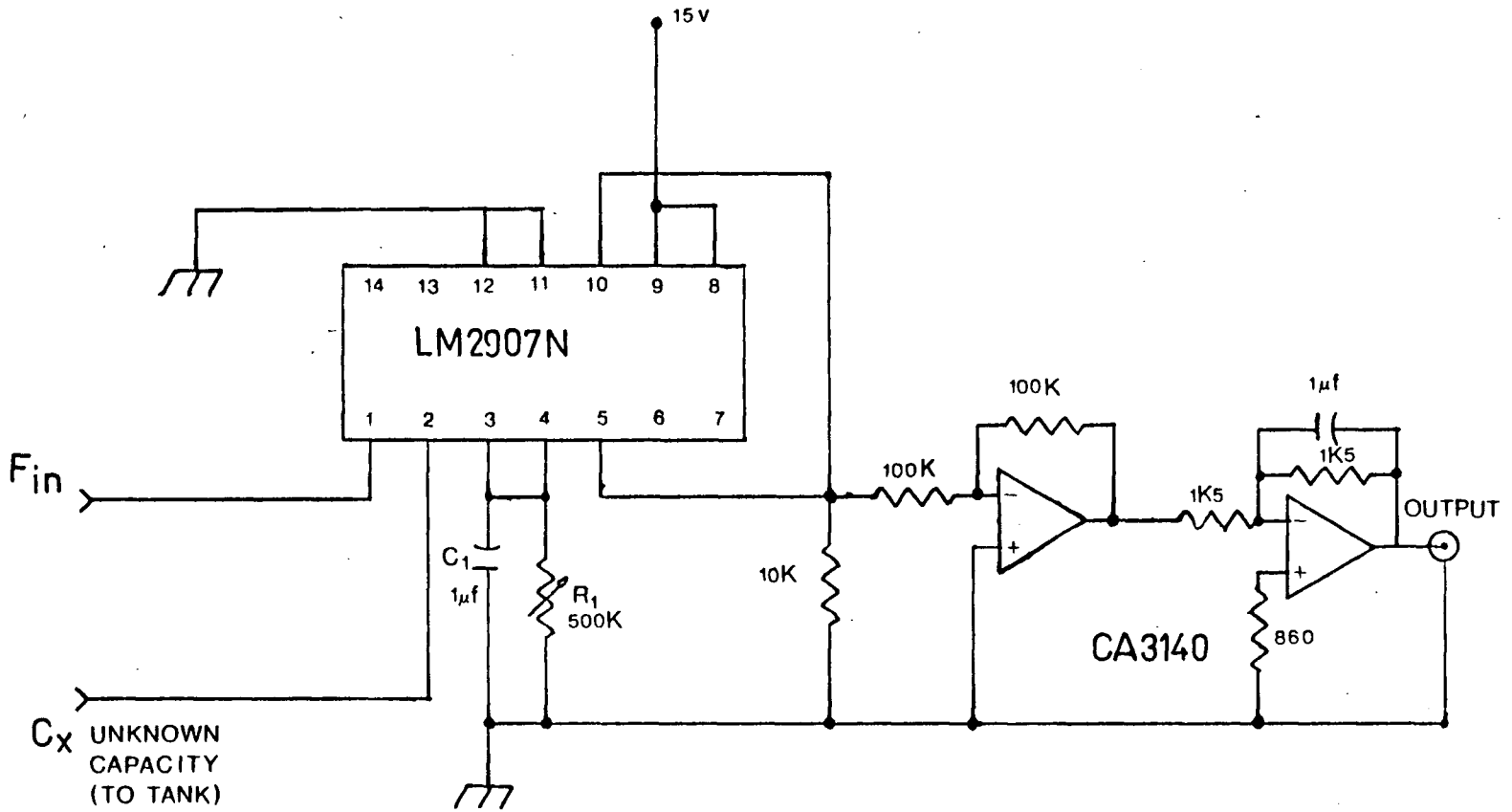

Figure 8. The I.C. capacitance measuring circuit.

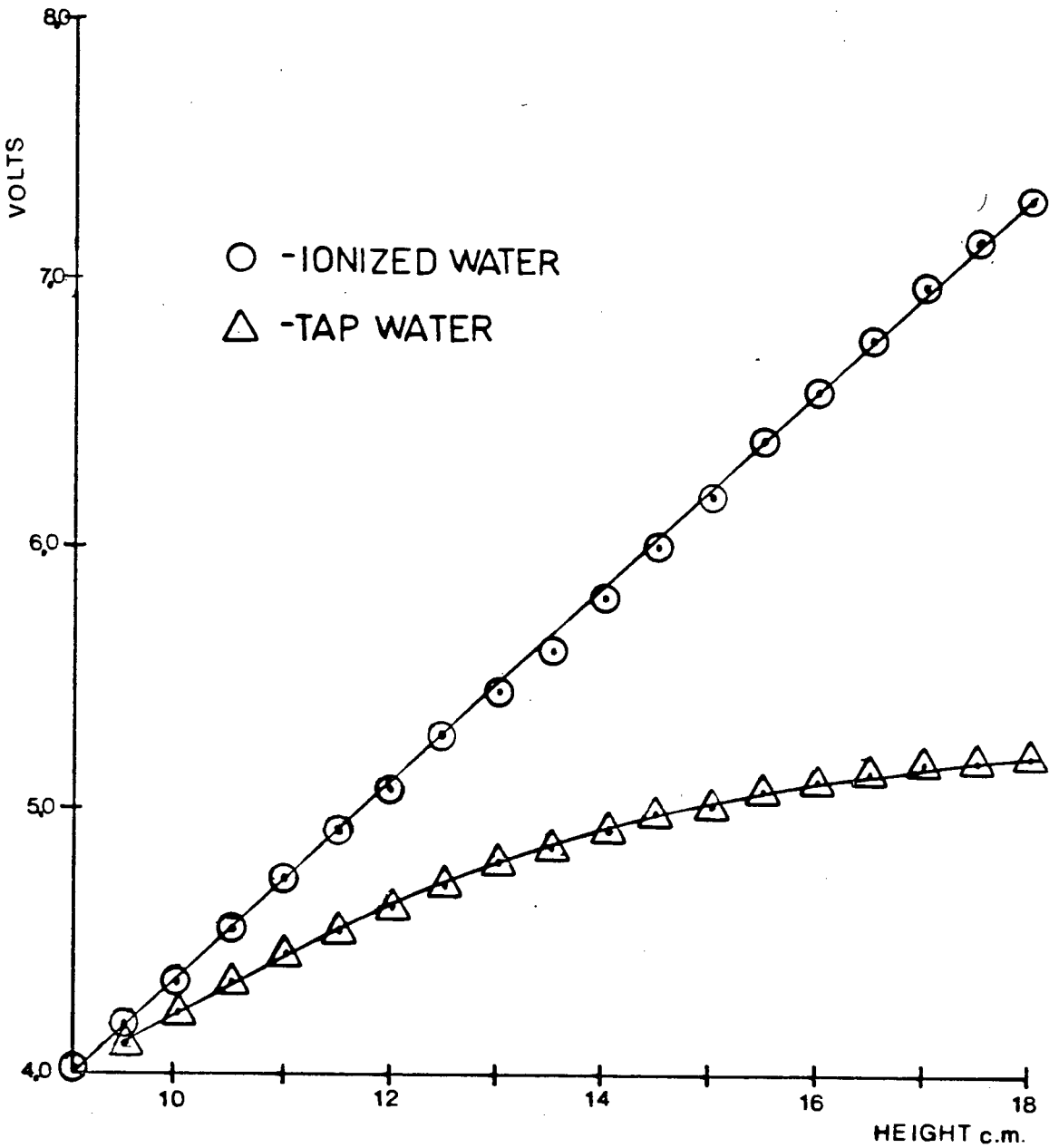

Figure 9. Response of the I.C. capacitance measuring circuit to changes in water depth.

CHAPTER III

EXPERIMENTAL RESULTS

A. Capacitance Measurements

Duplication of the original experimental set-up devised by Langille (1970) yielded results that appeared at first inspection to be in accordance with the general theory. The arrangement used distilled wter as the dielectric between two Varathane varnish covered Fourier analyzing plates. As shown in Figure 10, the output signals from the impedance bridge appear to be exponential with time and are larger for runs with an initially perturbed surface than for an unperturbed surface. Because of spurious electrical noise problems, I replaced the the electrostatic wave generator by a pulsed air jet which excited the second harmonic (q = 2) wave as the initial perturbation. However, this method of wave excitation results in waves which are rather rich in harmonic content as Figure 11 shows. Plotting the results for each mode versus $\cosh(\omega_i t)$ where ω_i is the angular frequency of the particular mode analyzed, yielded curves that do not deviate significantly from staight lines at early times (Figure 12).

To eliminate the noise problems caused by the electric field of the wave generator, I rebuilt Langille's apparatus using the water as a capacitor plate and a

a)

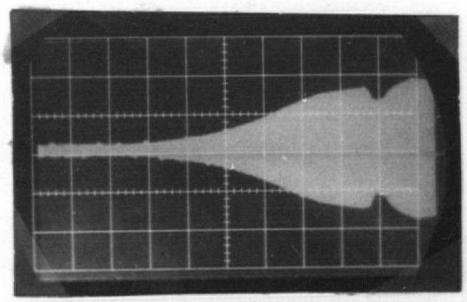

b)

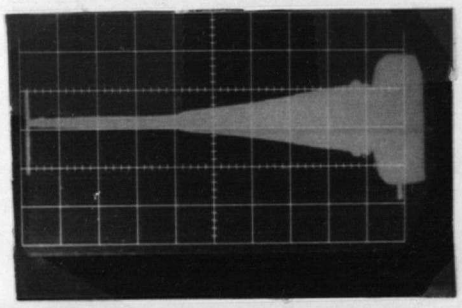

Figure 10. Output of the impedance bridge as a function of time.
a) Growth of a perturbed surface.
b) Growth of an unperturbed surface.
Gain is 0.1v/div, time base is 20 msec/div.

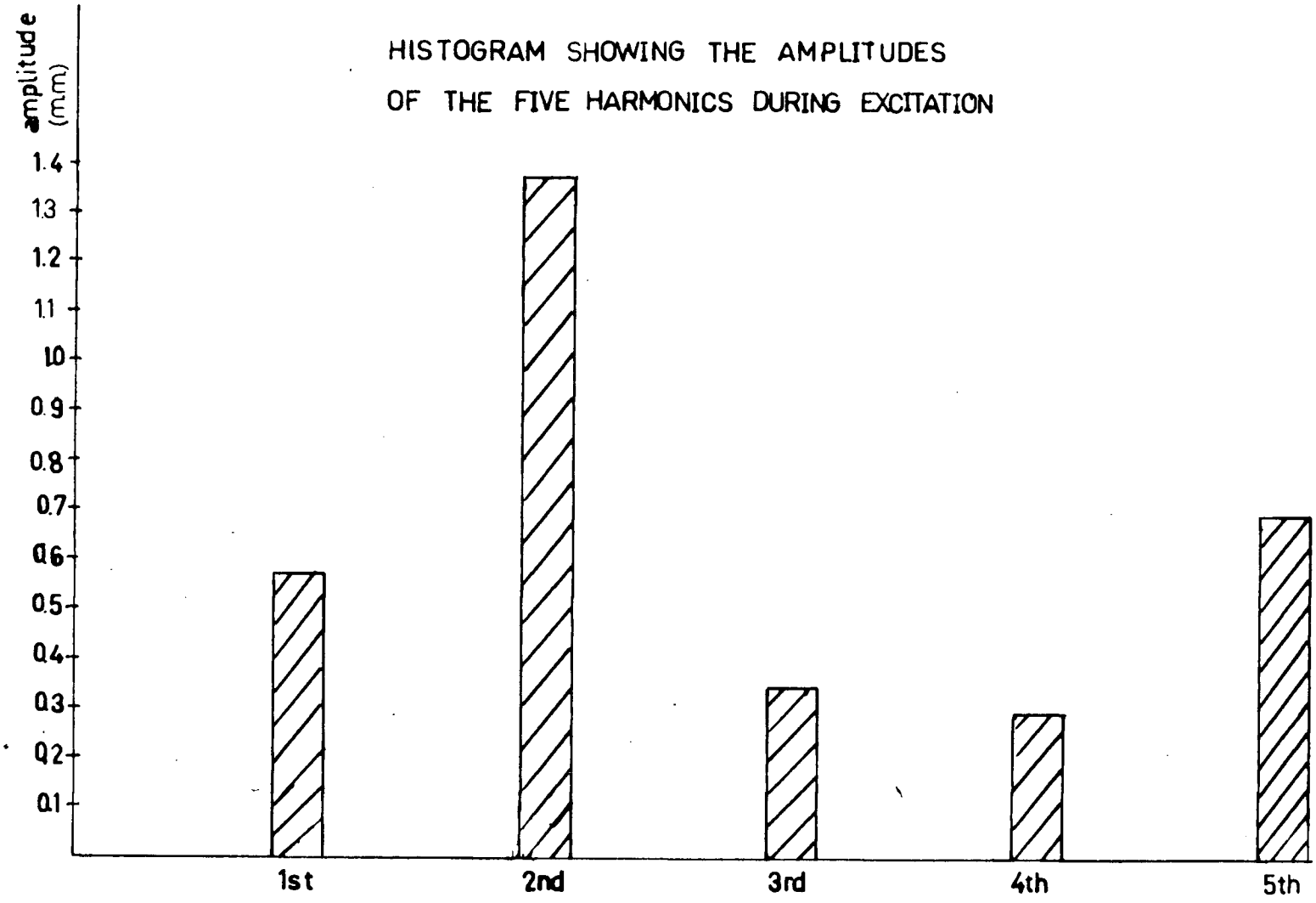

Figure 11. Spectrum of the second harmonic wave generated by a pulsed air jet. The horizontal axis is number of the qth harmonic of the Fourier analyzing plate used to detect the waves.

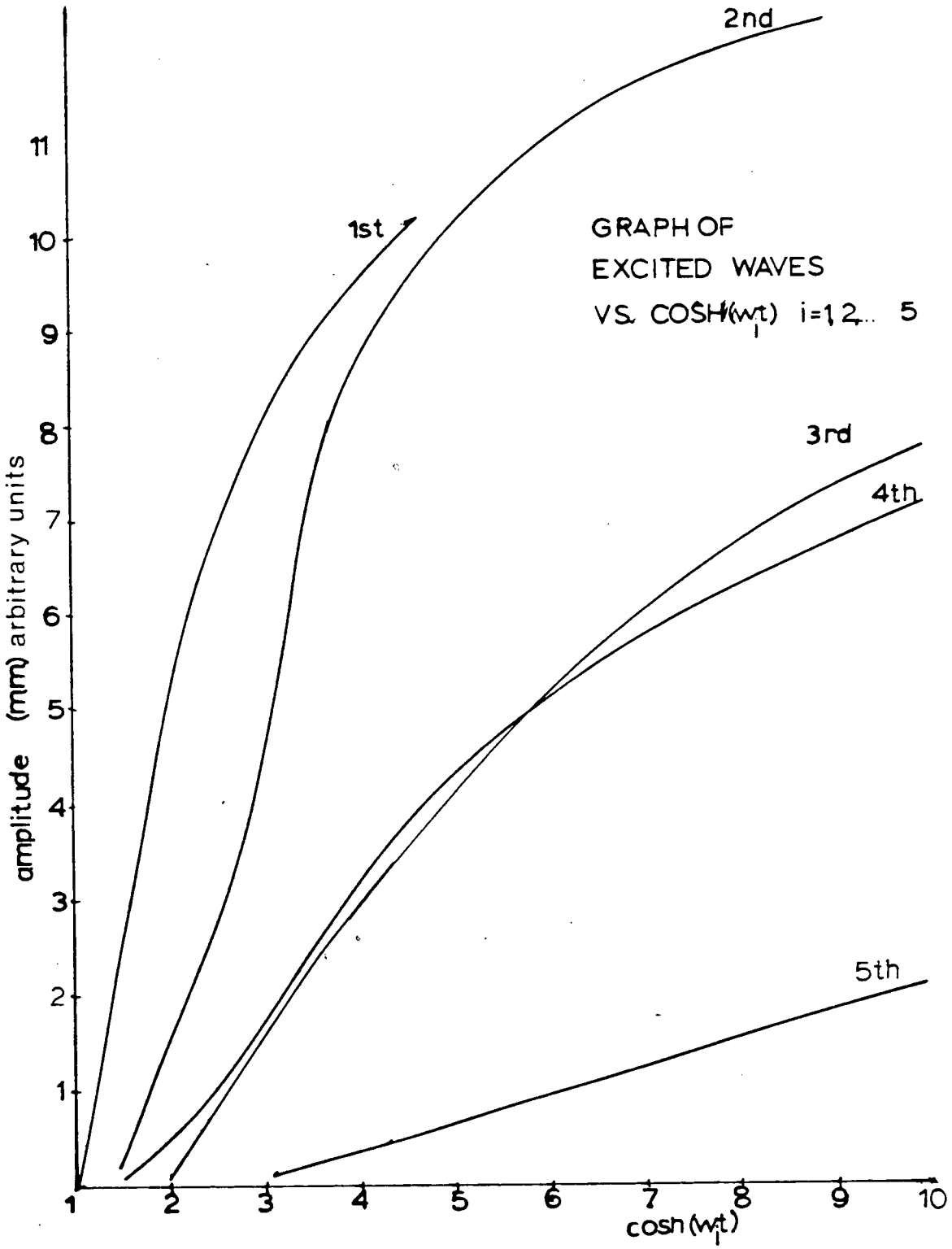

Figure 12. Results using the water as a dielectric. The output signals obtained by using different harmonic plates are plotted versus $\cosh(\omega_i t)$ where $i=1,\ldots 5$.

0.077mm thick polyethylene sheet as the dielectric as described in Chapter II part B. Initially, all experiments were performed using the first harmonic standing waves as the initial perturbation since the aim of the experiment was to follow the development of higher order modes due to the distortion of the growth of a lower order mode.

The impedance bridge used in these experiments is the General Radio 1500-A. For optimum results, the sensitivity control of the bridge was set a the 9 o'clock position, the CRL selector switch was set at "C_s" and the DQ dial is typically set at ≤ 0.1 (on the "low D" scale) for balance. When runs were made using the impedance bridge, it was found that the growths were no longer exponential as they were in Langille's set-up where the water was used as the dielectric. Also, it was seen that the effect of "phasing" (i.e.,releasing the tank when $\phi = 0, \pi$ or $\pi/2$ in $\eta = A\cos(\omega t + \phi)\cos(kx)$), has negligible effect on these growths as in Figure 13.

These results were confirmed when the I.C. capacitance measuring circuit was used in place of the impedance bridge.The striking feature of these results is the fact that that the capacitance decreases in a non-exponential fashion in all cases irrespective of the phasing of the initial perturbation, (Figures 14a) and 14b)) .

a)

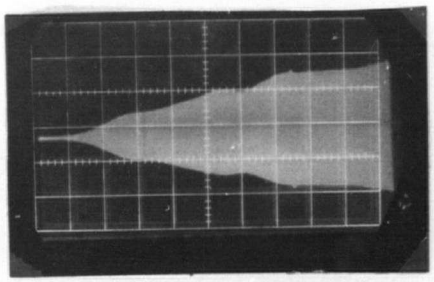

b)

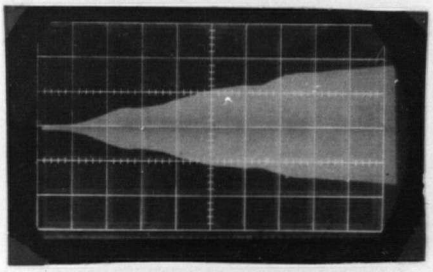

c)

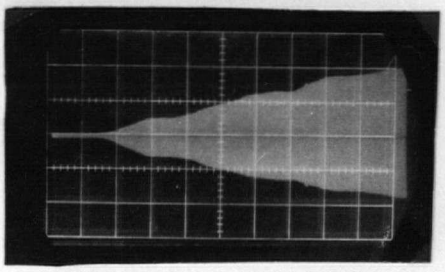

Figure 13. Impedance bridge output versus time showing that the growth rate of the instability is independent of the phase, Φ.

a) Phase $\Phi=0$
b) $\Phi=\pi/2$
c) $\Phi=\pi$

Gain is 0.1v/div Time base is 20 msec/div.

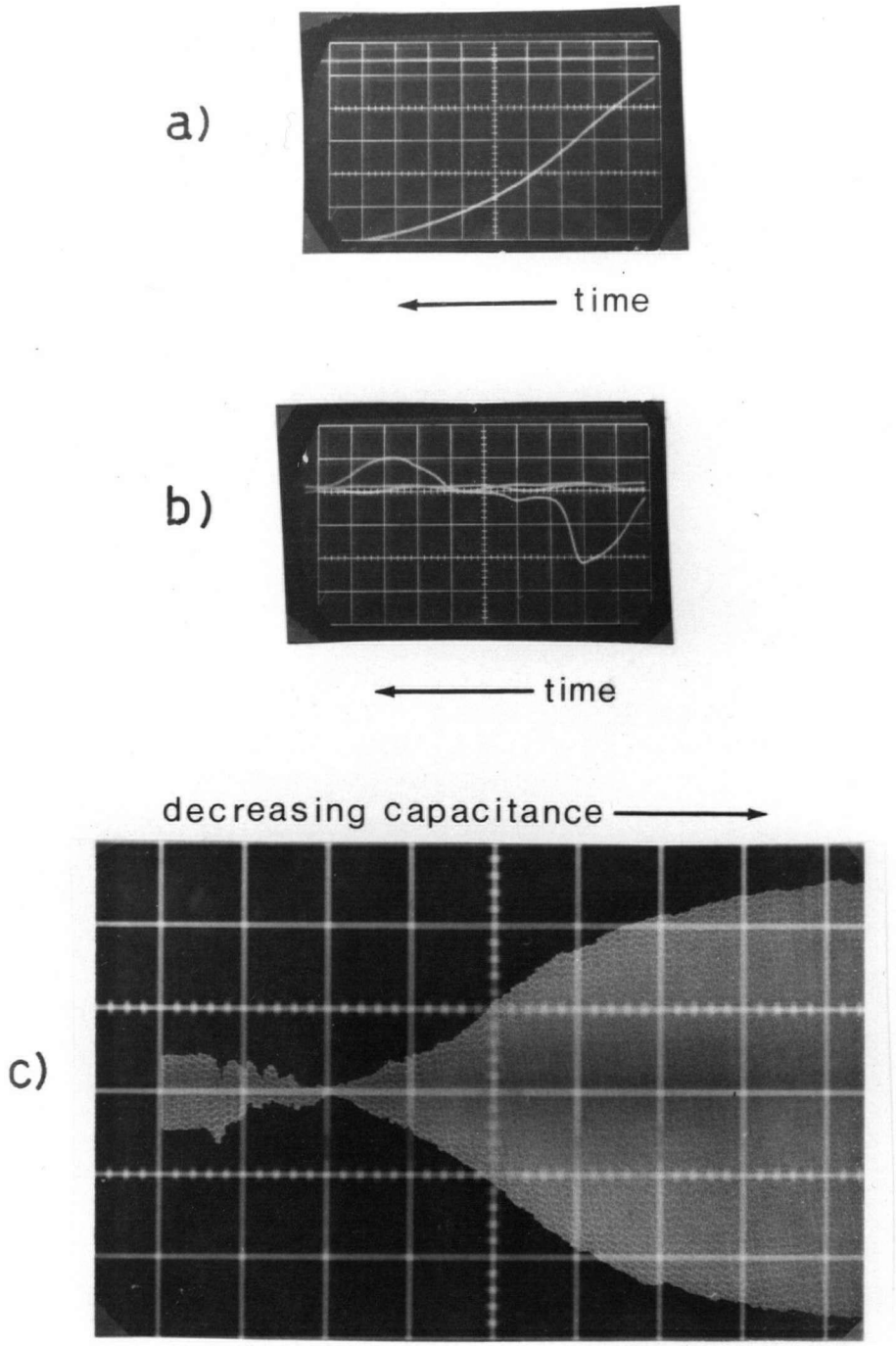

Figure 14. Capacitance measurements showing the decrease in mean level caused by the growth of instabilities.

a) I.C.circuit output,gain is 0.2v/div, time base is 20 msec/div.
b) I.C. circuit output,gain is 0.5v/div time base is 0.2sec/div.
c) Capacitance bridge output,gain is 0.1v/div and the time base is 20msec/div.

The direction of the growth was later verified using the impedance bridge. This was done by setting the reference capacitance on the impedance bridge below that of the tank with the unperturbed water in it. This of course, results in an output signal that is appreciably greater than the null balance signal. When the tank was accelerated downward, the output is seen to decrease to the null signal level once the capacitance of the tank has diminished to that set on the impedance bridge. A further reduction in capacitance then causes the output to grow with time, (Figure 14c)).

The results from the impedance bridge and I.C. circuit suggest that there is a change in the mean level of the contact of the water with the walls of the water tank. Because the capacitance decreases with time, it would then seem that water is separating from the walls and hence the mean level decreases.

B. Resistance Measurements

Observing the voltage signal between two Fourier analyzing plates immersed in ionized water yielded rather surprising results when the tank was accelerated downward. Since the area of contact with the walls is expected to increase due to the growth of the instability, the voltage between the plates should correspondingly decrease since it is inversely proportional to the area. However,

as seen in Figure 15, the voltage increases in an exponential fashion. Using the 1st harmonic wave as the initial perturbation, semi-logarithmic plots of the amplitude versus time yielded linear graphs whose slopes then gave the growth rate. It was found that using the various harmonic plates produced approximately the same growth rate. The results are presented below:

TABLE III : RESISTANCE FOURIER ANALYSIS

HARMONIC NUMBER (q)	GROWTH RATE η (sec^{-1})
1	23.5 ± 13%
2	23.4 ± 14%
3	23.4 ± 15%
4	25.4 ± 17%
5	19.8 ± 18%
plain copper sheet	20.7 ± 11%

The growth of the voltage signals in the opposite direction of that expected can be explained by assuming once again that the area of contact of the water with the walls decreases linearly with time as the capacitance observations indicate. Since the inverse of a linearly decreasing function is a rising hyperbola, the voltage signals which are proportional to the inverse of the contact area then appear as positively going exponentials.

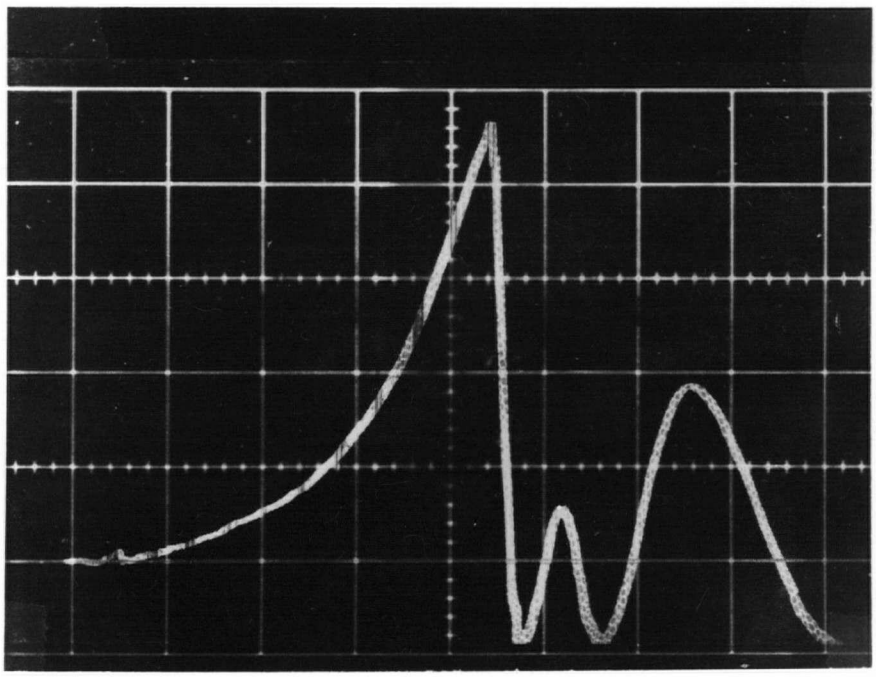

Figure 15. The resistance Fourier analysis. Voltage across the tank as a function of time.
Gain is 0.05v/div and the time base is 50msec/div.

The voltage signals observed here can be used to interpret the exponential growths that are observed when the water is used as the dielectric between two Fourier analyzing plates. In this configuration, (Curzon and Langille 1972) , there is considerable leakage of current across the tank since the water and the varnish on the capacitor plates are ineffective as insulators. Thus, it is the resistance between the plates that is actually being measured by the impedance bridge and hence the exponential growths are obtained. Langille (1970) notes that there is difficulty in maintaining the null balance signal constant and low from one experimental run to the next. However, when the tank is used as a proper capacitor (see Figure 4) , there is no problem to balance the bridge to obtain a null signal of less than 1 mV r.m.s.

In summary, the resistance and capacitance measurements yield unexpected results. The fact that the resistance increases and the capacitance decreases as the tank is accelerated indicates that there is a change in the mean level of the water that is in contact with the walls. Thus, the measurements do not give an indication of the instability but describe the situation at the walls of the container.

C. "Cavitation" Effects

Irrespective of the mode initially on the surface, the signals from the impedance bridge always indicate a linear growth due to a decrease in capacitance. Since the capacitance measured is averaged over the area of the plate

$$C = \int (\varepsilon/d)\, dA$$

the only way that the capacitance can decrease is if d, the separation between the two capacitor plates increases. This means that if the water pulls away from the walls so that air gets between the water and the polyethylene sheet, d will increase and the capacitance will be seen to decrease. If the thickness of the air film is large compared to the thickness of the dielectric sheet, then

$$C = \int_{A'} (\varepsilon/d)\, dA'$$

where A' is the area of the water in contact with the dielectric sheet. If the other plate of the capacitor is a metal sheet, then the above expression indicates that C will be proportional to the average depth $\overline{D}$ of the water which touches the dielectric of the capacitor. For given applied virtual acceleration, it was observed that dC/dt (i.e. $d\overline{D}/dt$) is constant. The possibility that this phenomenon is the same as the formation of the bubbles of the instability can be eliminated since

others (Emmons et al 1959), have found that the bubble velocity is proportional to the square root of the virtual acceleration. For convenience, this apparent replacement of water by an air film will henceforth be called "cavitation".

To determine how the cavitation phenomenon is affected by the initial shape of the surface, experiments were performed where an adjustable Plexiglas baffle was placed in the tank. The baffle was vertical, with its plane parallel to the capacitor plate. The distance of the water between the capacitor plate and the baffle was varied from 0.5 cm to 10.5 cm. At 0.5 cm there is considerable curvature of the water surface due to the meniscus.

Investigations were performed with no excited waves on the initial water surface. The cavitation rates were determined simply by measuring the slopes obtained from the bridge signals (Figure 16). The sensitivity of the capacitance bridge was established by slowly filling the tank and observing the output voltage as a function of water depth. The sensitivity was 6.67cm/V_{p-p} and was observed to be linear to a net change of 9cm of water provided that the sensitivity control on the bridge is maintained at one quarter of a turn or less (Figure 17).

A typical graph of the measured cavitation

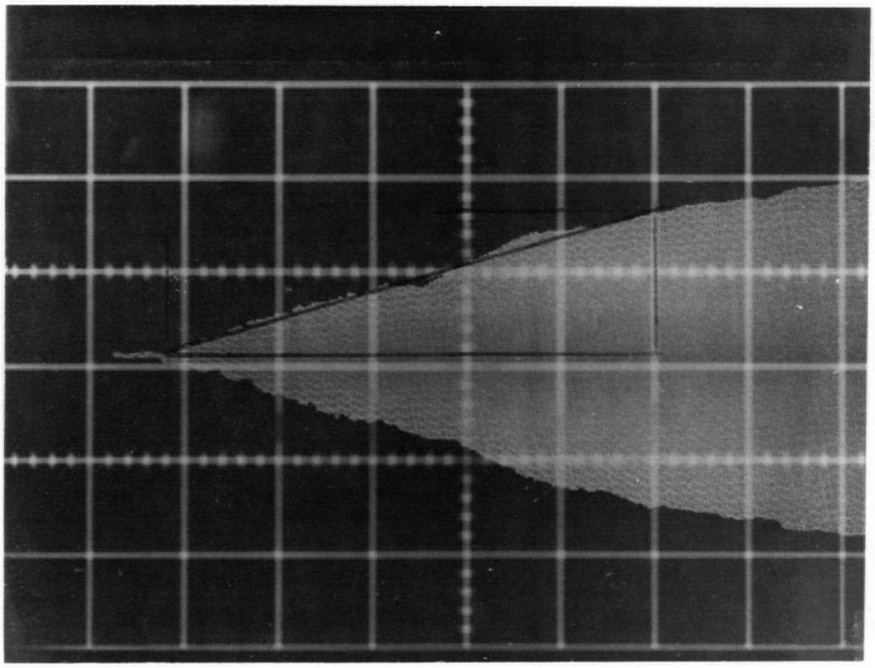

Figure 16. Oscillograph showing the linear decrease of tank capacitance with time. The tank width was 2 cm in this instance and the virtual acceleration 1.0 g's. Gain is 0.2v/div, time base 20msec/div. The calibration is 6.67cm water/V_{p-p}.

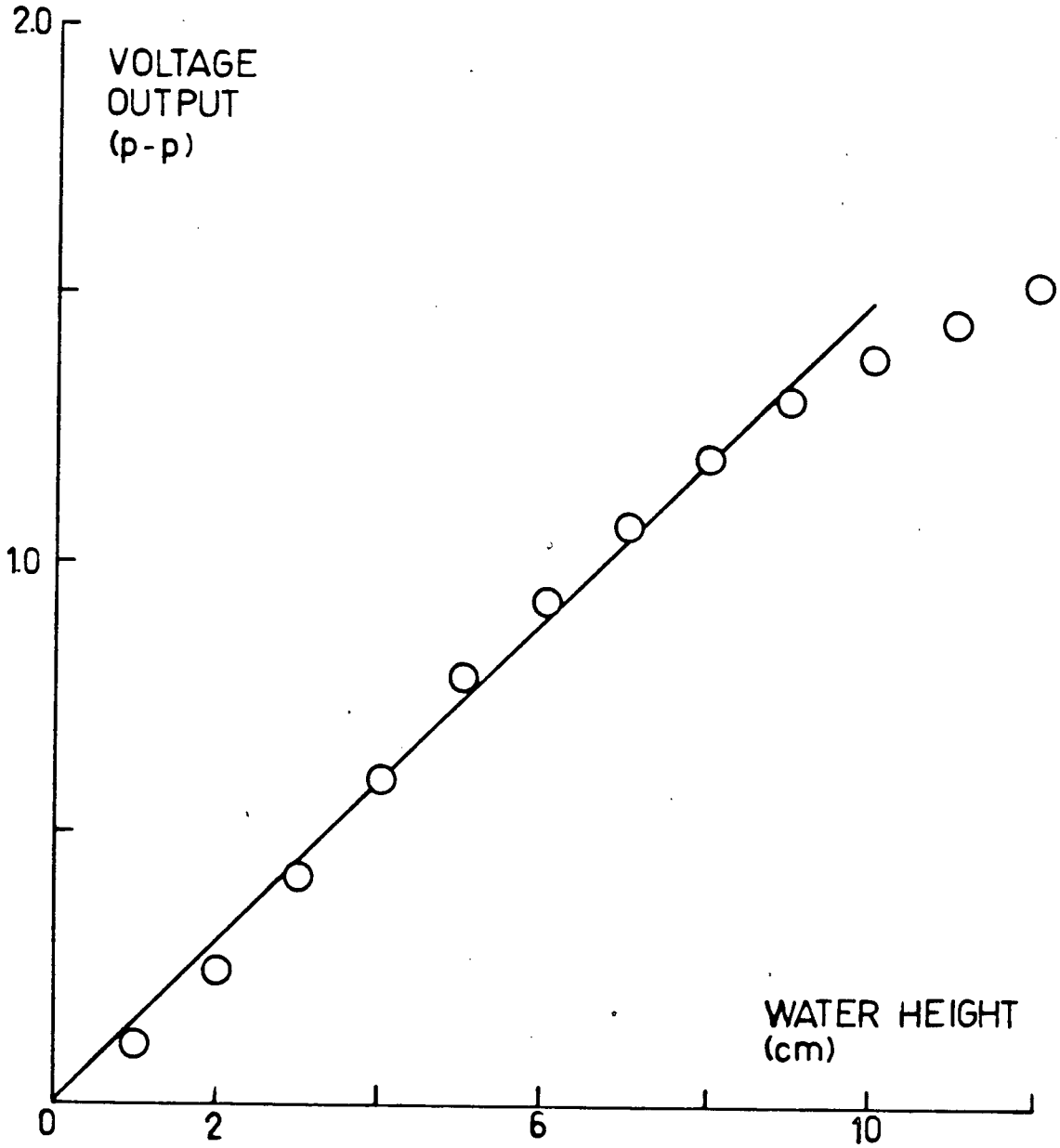

Figure 17. Calibration of the GR-1500A impedance bridge. Water height is measured upwards from the equilibrium level.

velocity ($d\bar{D}/dt$) as a function of virtual acceleration is shown in Figure 18. The error increases for the larger accelerations because the growth is observed for considerably shorter times and there is also an increase in spurious noise signals in the envelope of the bridge output. The results for the investigation of the effect of the tank width are presented below:

TABLE III : CAVITATION RATE AND TANK WIDTH

TANK WIDTH (cm)	RATE (cm/sec-g)
0.5	37
1	30
2	38
3	32
4	39
6	27
8	34
10.5	32

As seen from table III, there is no observable dependence of the cavitation velocity on the tank width; the net result is that the velocity of the decreasing mean level is related to the virtual acceleration by:

$$d\bar{D}/dt = v = (34\text{cm/sec-g} \pm 4\text{cm/sec-g}) \times g$$

where g is the virtual acceleration or excess acceleration

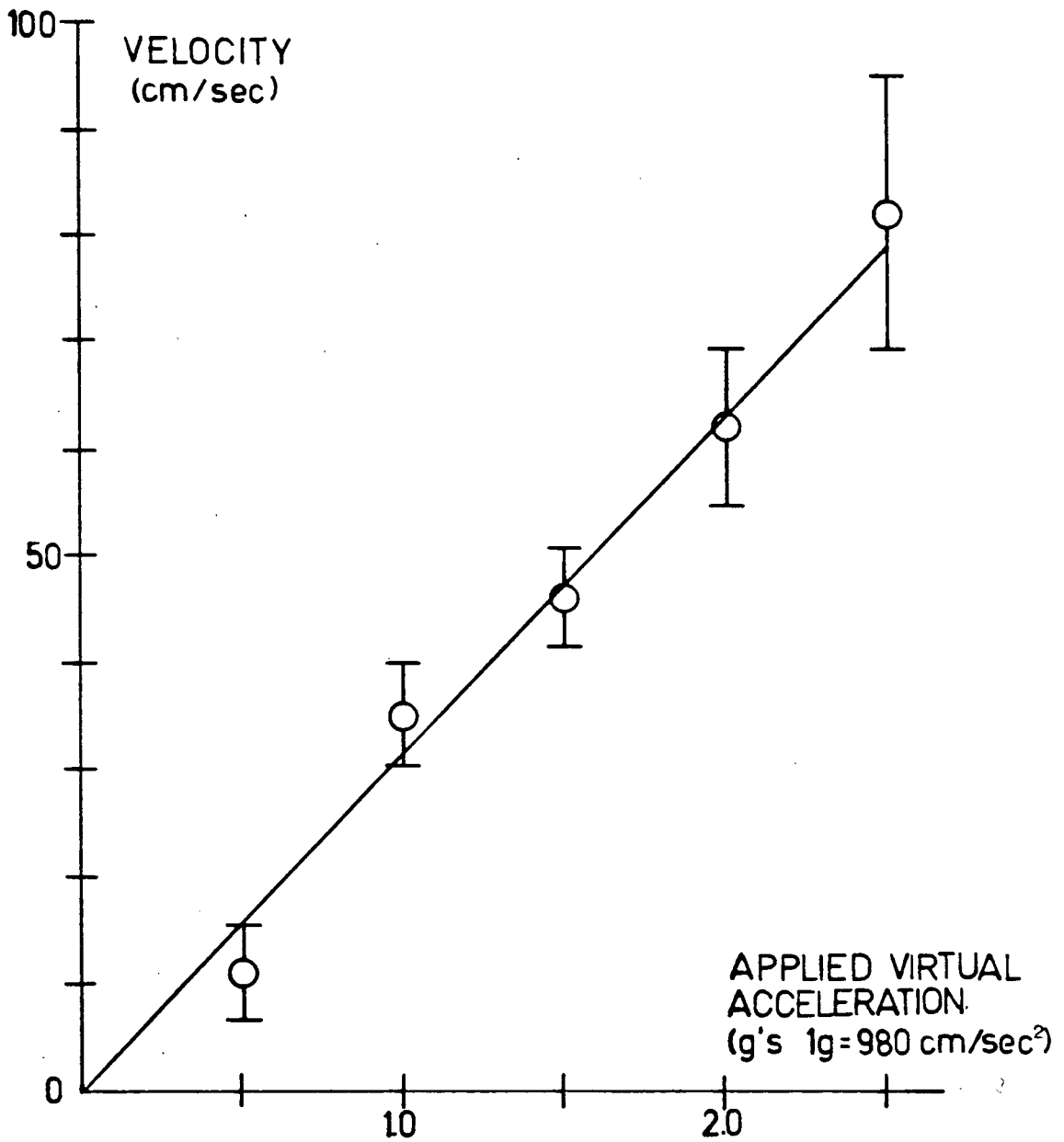

Figure 18. "Cavitation" rate for a tank width of 3 cm.

in terms of free fall acceleration i.e., $g = \alpha g_o$, $g_o = 980\ cm/sec^2$, $\alpha > 0$.

Dimensional inspection of the proportionality between the velocity and the applied acceleration leads to scaling laws, from which the dependence of the cavitation rate on various physical quantities may be deduced. In particular, when the constant of proportionality was considered as being a function of the density and viscosity, the dimensional analysis yields the plausible result that the cavitation rate should be inversely proportional to the viscosity:

$$\frac{d\bar{\Pi}}{dt} = v = \frac{\rho g L_o^2}{\eta}$$

where L_o is a scaling length and η the viscosity.

To check the viscosity effect, aqueous sugar solutions were prepared of different concentrations ranging from 20 to 60 percent sugar by weight. The viscosities of these solutions at 25°C is given by the Handbook of Chemistry and Physics, 43rd edition and are listed in table IV together with the experimental results:

TABLE IV : EFFECT OF VISCOSITY ON THE CAVITATION RATE

PERCENT SUGAR (by weight)	VISCOSITY (cP)	CAVITATION RATE (cm/sec-g)
20	1.695	32
30	2.735	31
40	5.164	46
50	12.40	35
60	44.03	77

From the table it is immediately apparent that the cavitation rate does not vary inversely with the viscosity as supposed. The rates above yield a mean value of 44 cm/sec-g with a standard deviation of 17 cm/sec-g so that the rates of the viscous solutions are comparable to those for pure water.

The large scatter in the data for the sugar solutions is due to the erratic irregularities of the bridge signals that appear at accelerations greater than 1.5 g. The rates were determined by drawing the best fit line through the points as in Figure 19 . This necessitated the exclusion of the origin at 0 acceleration. Nonetheless, even if the origin is included in the dtermination of the cavitation rates, the conclusion still remains that there is no inverse variation with viscosity.

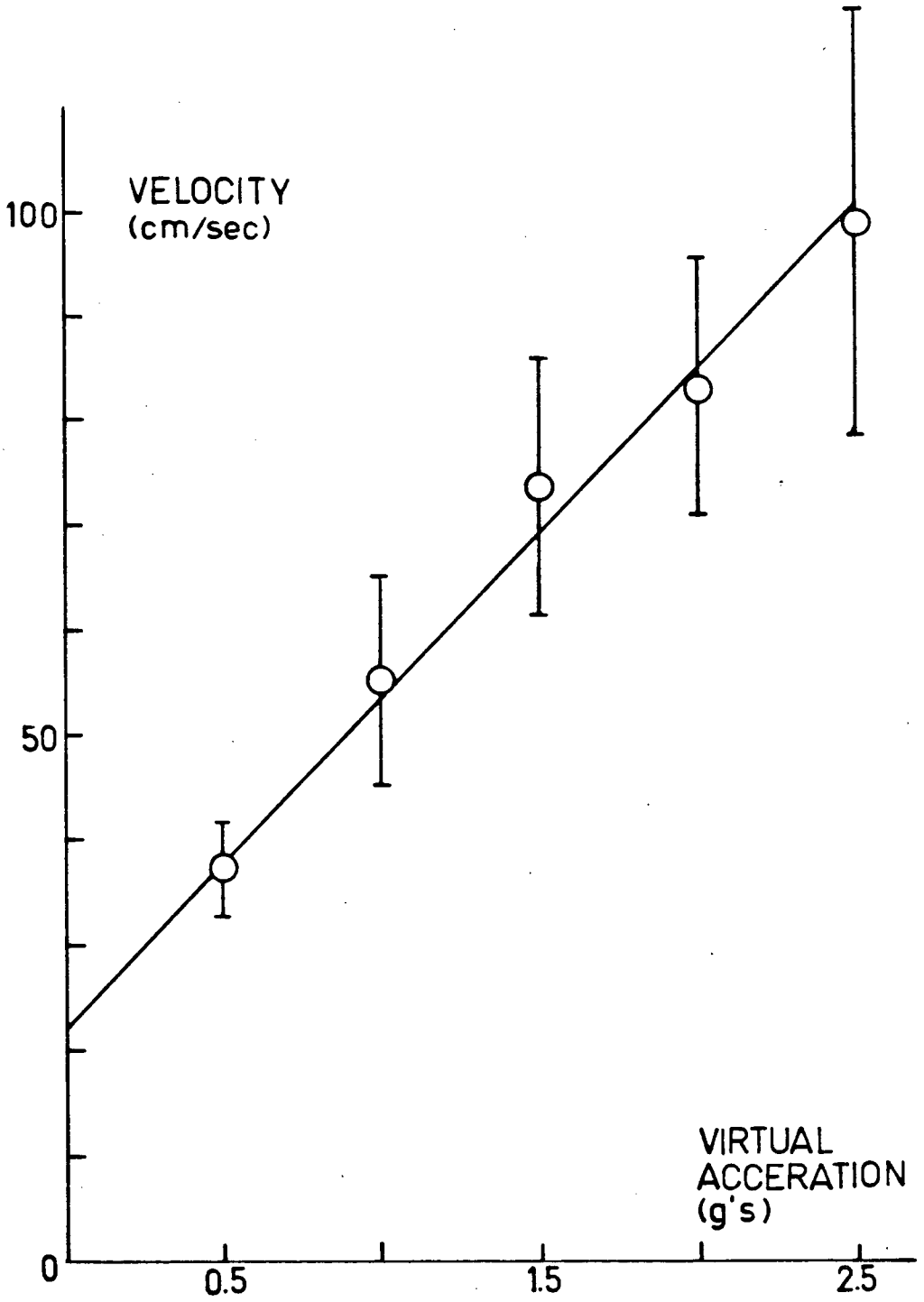

Figure 19. Cavitation rate versus the virtual acceleration for a 30% sugar solution.

The response of the bridge to transient changes in capacitance was checked to ensure that the linear growths obtained in the runs are truly representative of the physical situation and are not due to some inability of the bridge to follow fast changes in capacitance.

One capacitor plate was fixed to the tank support frame and was held against the dielectric sheet and the other capacitor plate in the water tank. In this set-up, the maximum capacitance was 320 pF when the two capacitor plates fully overlapped one another. By dropping the tank, the capacitance was reduced to 250 pF when the two plates no longer had a common area of overlap.

Calibration of the signal output for this test gave a conversion factor of 11 mV/cm between the output amplitude and the relative vertical displacement of the capacitor plates. The tank was then allowed to fall, so that the capacitance of the two plates could be observed as a function of time. Plotting the amplitude against the time squared yield a staight line to an excellent approximation (Figure 20). The slope yields the value of 547 cm/sec^2 as the effective acceleration. Thus, one may safely conclude that the bridge does indeed accurately follow abrupt changes in capacitance.

In view of the unexpected results from the electrical measurements, I decided to photograph the

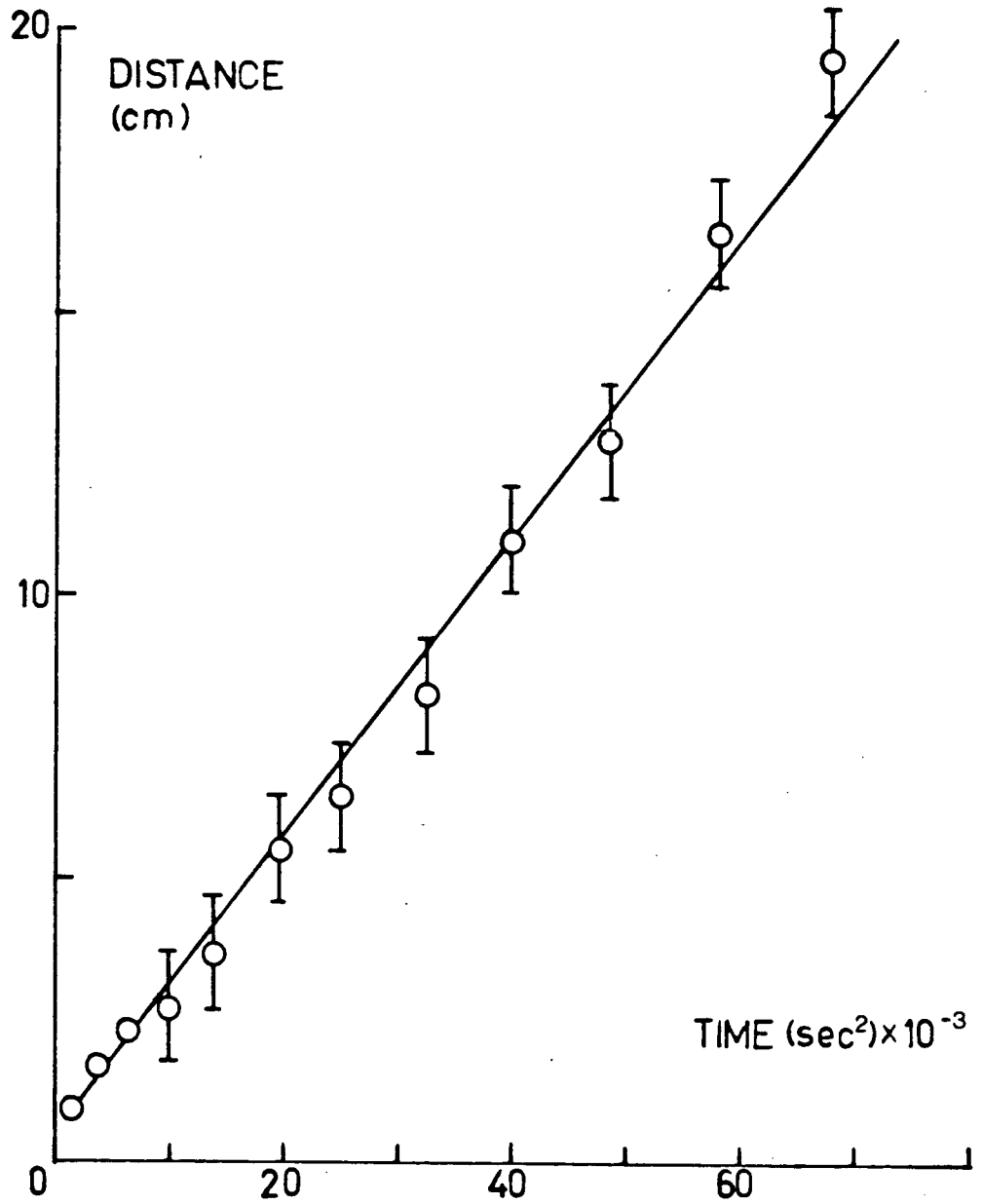

Figure 20. Test of the impedance bridge to transient changes in capacitance.

fluid motion in various ways so as to discover what sort of instabilities did occur and if an air film exists between the capacitor plates and the water in the tank.

D. Photography of the Fluid Motion

To determine visually the presence of instabilities, various modes were excited electrostatically on the water surface and the resulting instability was photographed. A mechanical switch located alongside one of the rails near the end of the tank's traverse, triggered a standard photographic flashgun aimed at the tank. The experiments were performed in total darkness and the camera shutter was held open throughout the duration of the run (500 msec or less). The instabilities were all photographed in their later stages of growth at the instant where they have reached maximum amplitude just before the motion of the tank is stopped by the shock absorbers. The photographs were all taken by a Nikormat EL camera with a 50 mm f/2 lens using Ilford PANF 50 A.S.A. film.

When the first harmonic wave was excited and the tank accelerated, it was found that there was negligible growth in the vertical direction and instead, most of the disturbance appeared across the tank (Figure 22a)). The photographs do show however, that there is a climbing

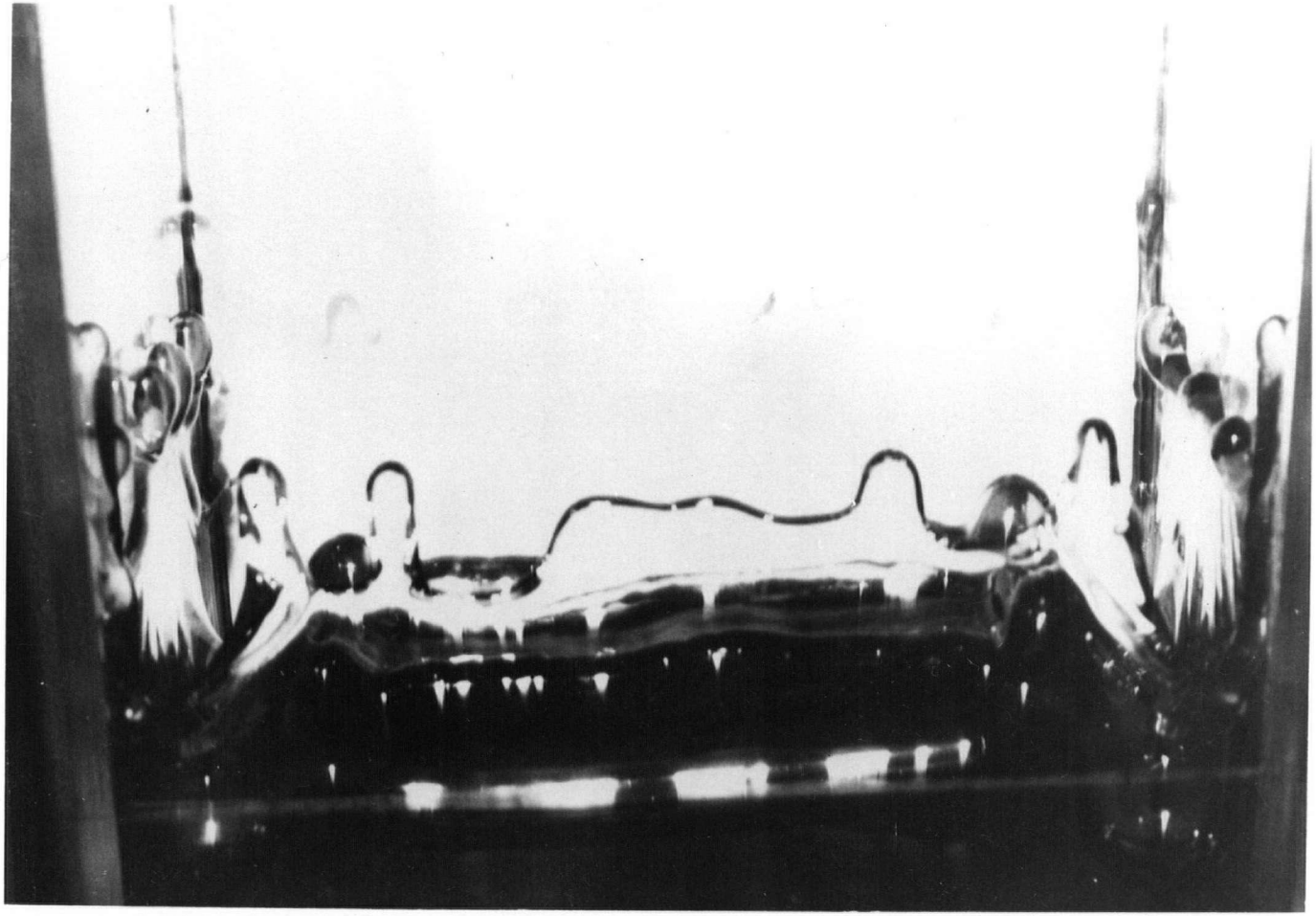

Figure 21. The initiall unperturbed surface at an acceleration of 1.5 g's.

film of water that bulges in the form of drops at the edges. This film exists on all four sides of the of the tank but is mostly seen on the side walls of the tank in the photograph. There is also the appearance of "bubbles" at the corners of the tank as was first noted by Emmons et al. Figures 21 and 22a) show that the disturbance of the unperturbed surface and that of the first harmonic excited wave respectively, are essentially the same. Therefore, the capacitance and resistance data obtained for the instability thought to arise from the first harmonic wave also apply to the initially unperturbed surface as well.

Photographs of the instability evolving from the second harmonic excited wave which was used by Langille (1970) show similar results as those obtained for the first harmonic wave (Figure 22b)). There is some growth in the vertical direction, but once again the transverse disturbance appears to dominate.

Successful instabilities were achieved when the 4th harmonic wave was excited using the electrode shown previously in Figure 5. Using the timing circuit described in Chapter II part D, reproducible 4th harmonic instabilities were obtained on each run (Figure 23). The effect of phasing was also successful in this case. The tank was accelerated at the instant when the excited standing wave had a phase of π or 0 and the results

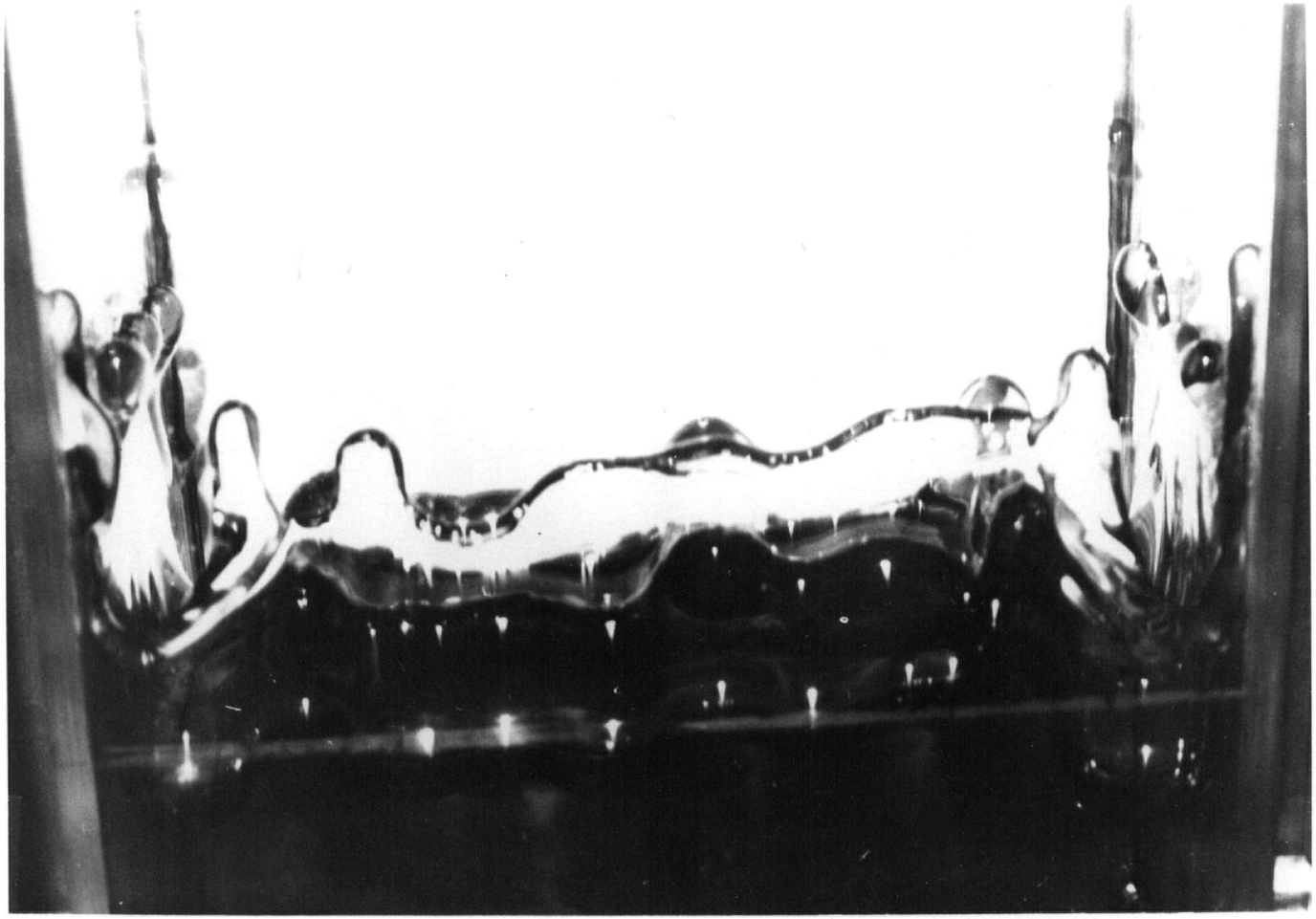

Figure 22. Flash photographs of the water surface.
a) The first harmonic excited wave at 1.5 g's virtual acceleration.

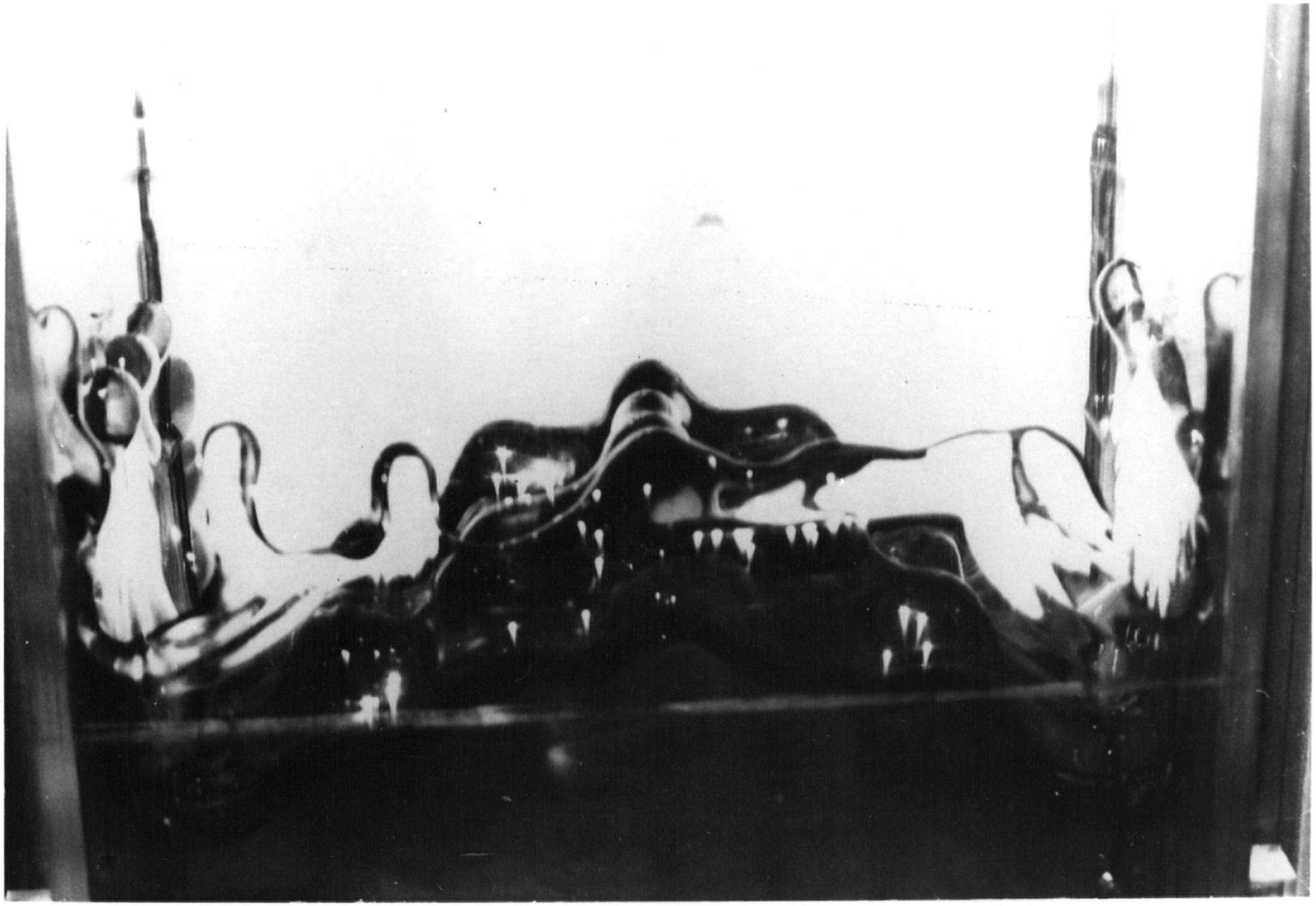

Figure 22. b) The second harmonic instability at 1.5 g's.

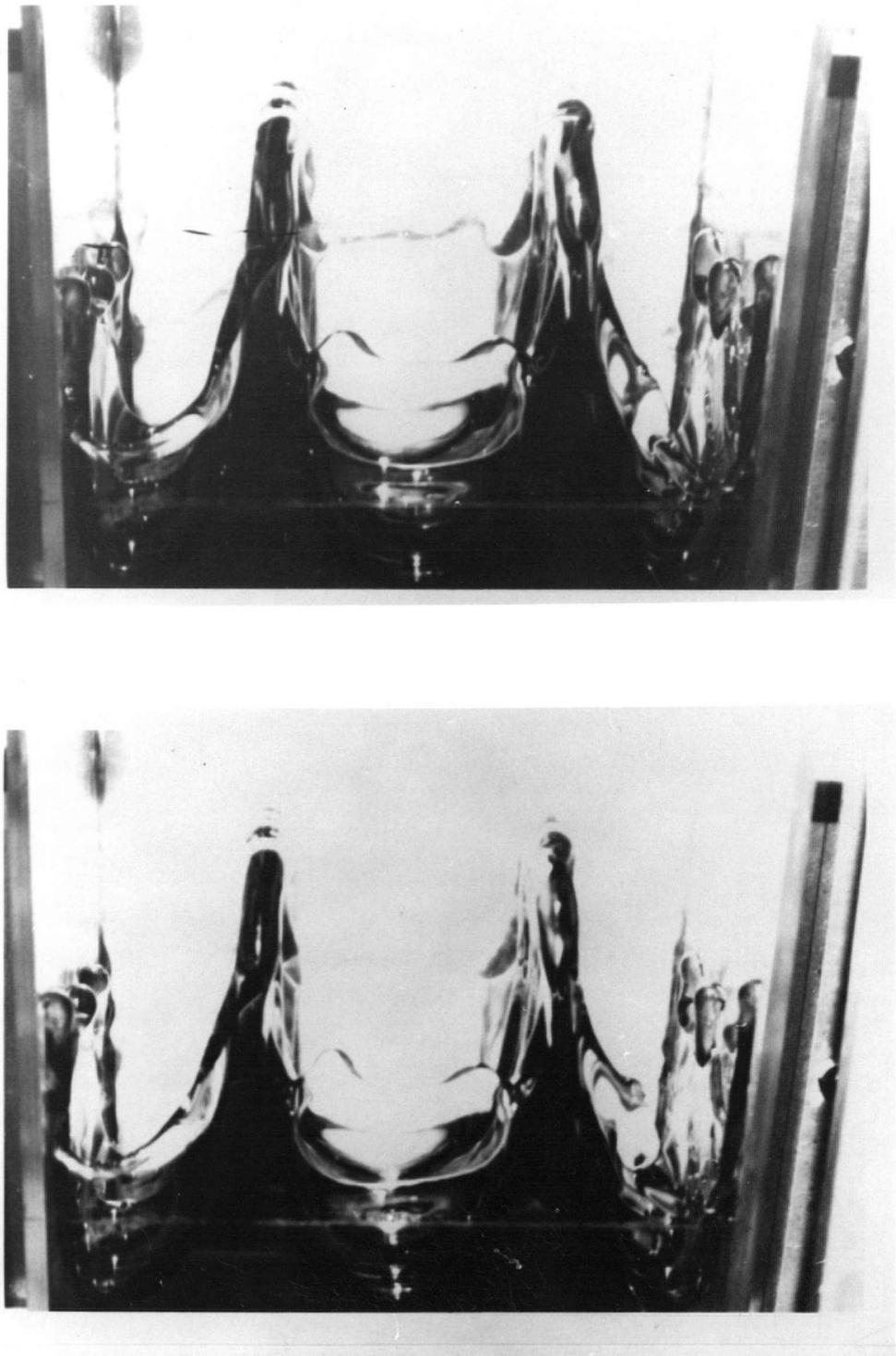

Figure 23. The fourth harmonic instability. The horizontal line in the photographs indicates the initial water level.The two consecutive shots indicate the degree of reproducibilty of the instability. The initial phase for these photographs was $\Phi=\pi$.

are as expected (Figures 23 and 24). The photographs indicate that the maximum amplitude attained by the spikes as measured from the initial water level is about 12 cm. In contrast, the initial perturbation has an amplitude of typically 1.5 mm.

In Figure 23, there is also seen some disturbance across the surface as well as across the top of the spikes perpendicular to the plane of the photograph. A photograph of the unaccelerated surface with the standing wave on it (Figure 25), indicates that a source of this transverse disturbance is due to some resonant excitation of a "cross-tank" mode along with the desired 4th harmonic along the length of the tank. Side-on photographs (Figure 26 a) and b)), indicate that there is a net tendency of the water to bulge outward in the middle of the tank whereas the water that is in contact with the walls is restricted in its motion because of its adhesion to the walls.

Further evidence that the contact area of the water with the walls lags behind the growth of the instability is provided by Figure 27. Here, the left half of the front wall of the tank has been fitted with a thin sheet of sandblasted Plexiglas. The sandblasted surface is in contact with the water and becomes dark upon being wetted by the coloured water.In all cases, the sandblasted side shows that the wetting due

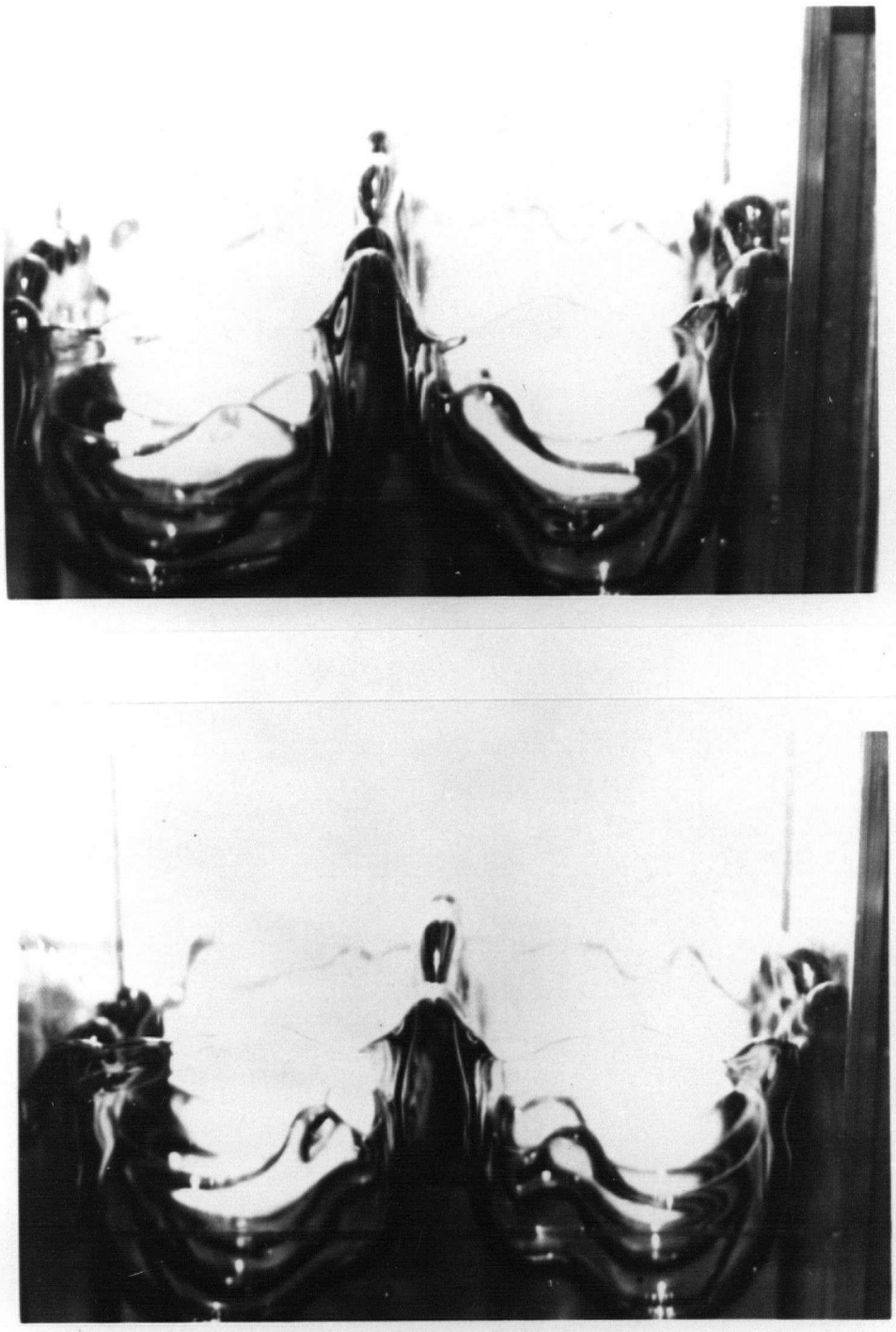

Figure 24. The same fourth harmonic instability as in figure 23, except that the tank was released when the phase of the standing wave was $\Phi=0$.

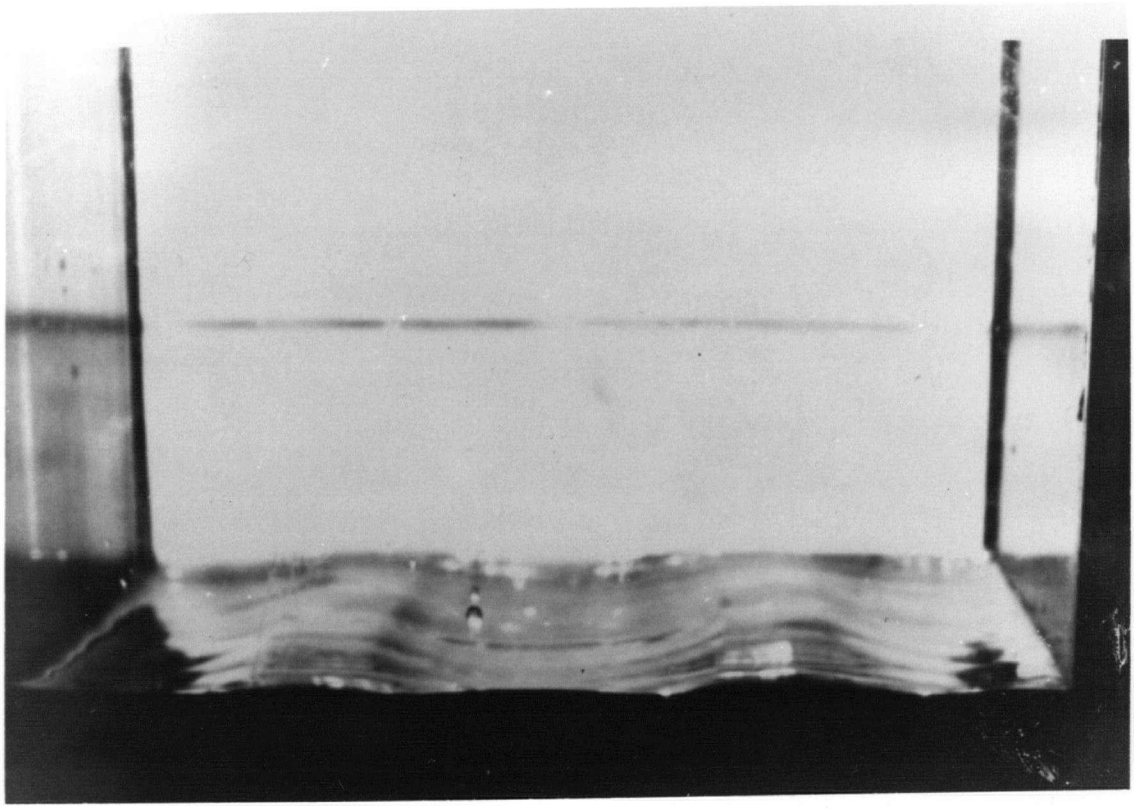

Figure 25. Flash photograph of the excited fourth harmonic standing wave at phase $\Phi=\pi$ in free fall.

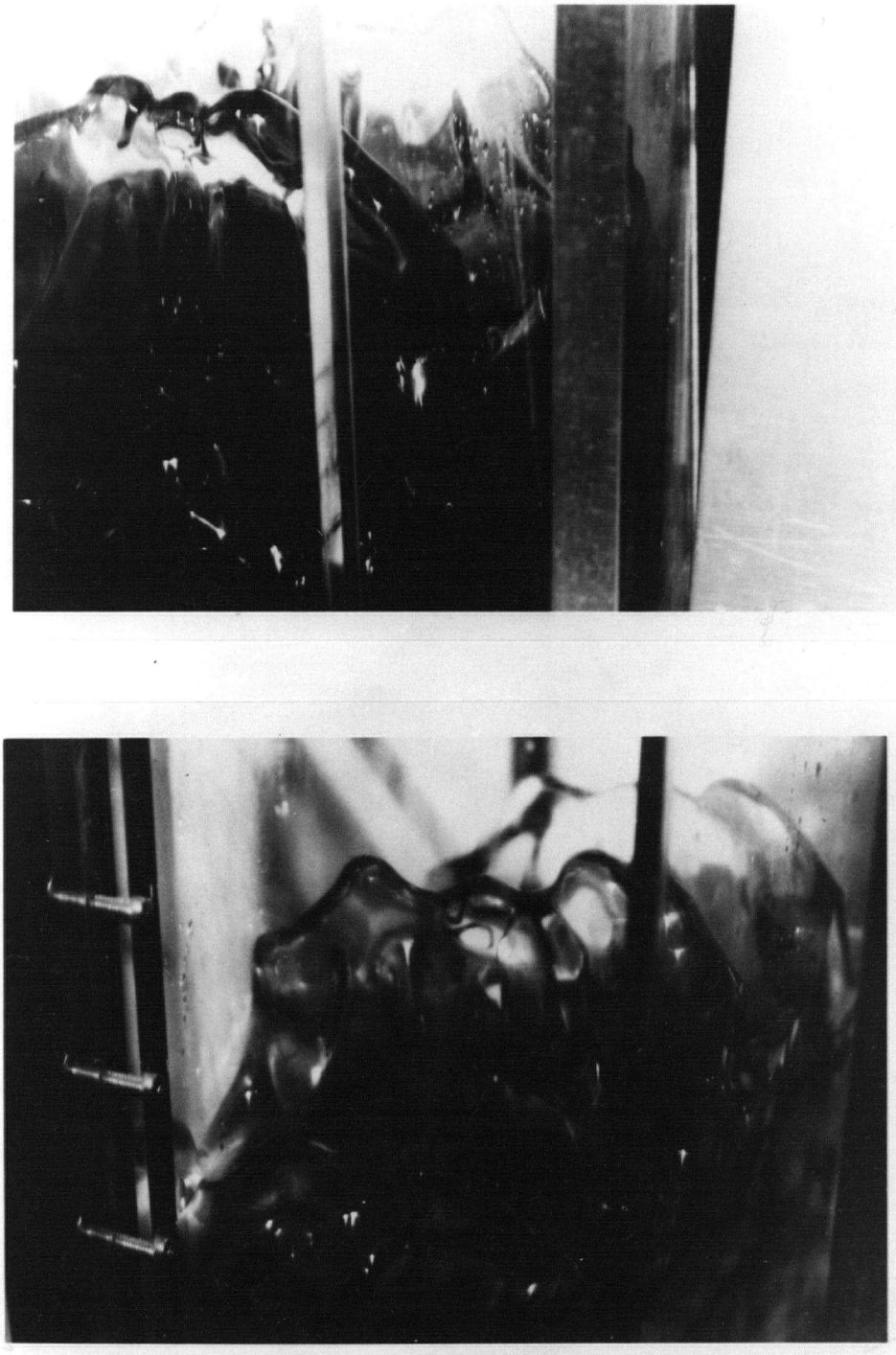

Figure 26. Side on flash photographs of the fourth harmonic instability showing the upward bulging of the fluid in the transverse direction across the tank.

a)

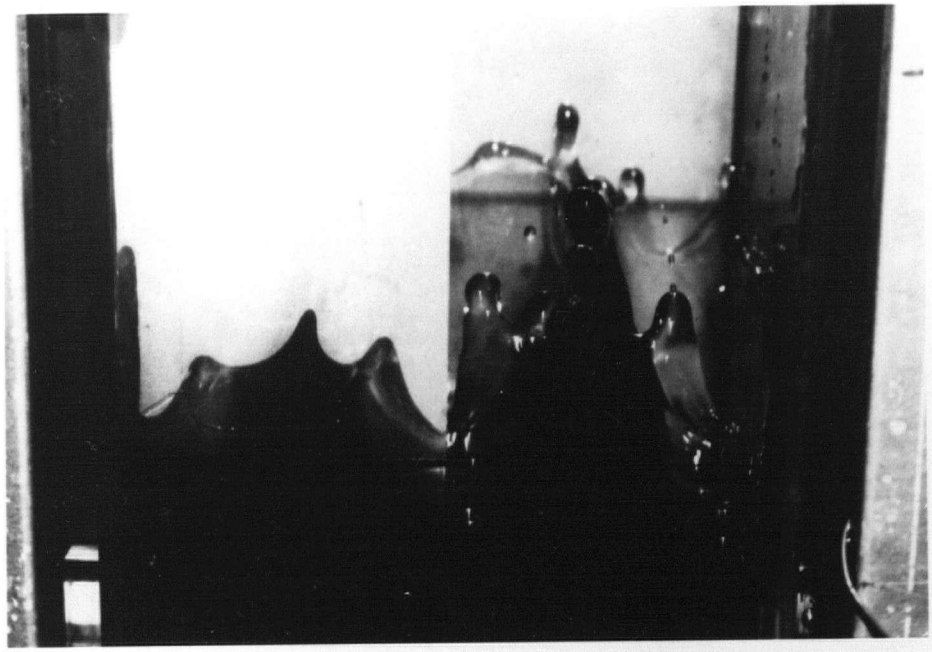

b)

Figure 27. The fourth harmonic instability with the left half of the tank showing the wetting of a translucent screen.

a) at 1.5 g's acceleration
b) at 1.0 g's.

to the growth of the spike is narrower and smaller than the spike which appears on the right hand side of the photographs.

Hence, in the tank of width 10.5 cm it has been seen that although the instabilities reach high amplitudes the water that is in contact with the walls does not follow the development of the instability. The tendency of the water surface to bulge upward must then necessarily pull in water away from the walls as the instability grows. Since the electrical measurements employed only measure the contact area of the water with a wall, they do not truly represent the growth of the instability, but instead indicate the apparently linear decrease of the contact area with time.

Lastly, the 8th harmonic mode was excited and the resultant instability observed. The motivation for exciting this high mode is that its wavelength approaches that used by the other investigators mentioned previously. It was found that the instability in this case does reach an appreciable amplitude (Figure 28), however the maximum amplitude achieved is about half that achieved by the 4th harmonic wave. In view of the complex structure and nature of the fluid surface for this particular mode, it was considered unprofitable to do further studies of it.

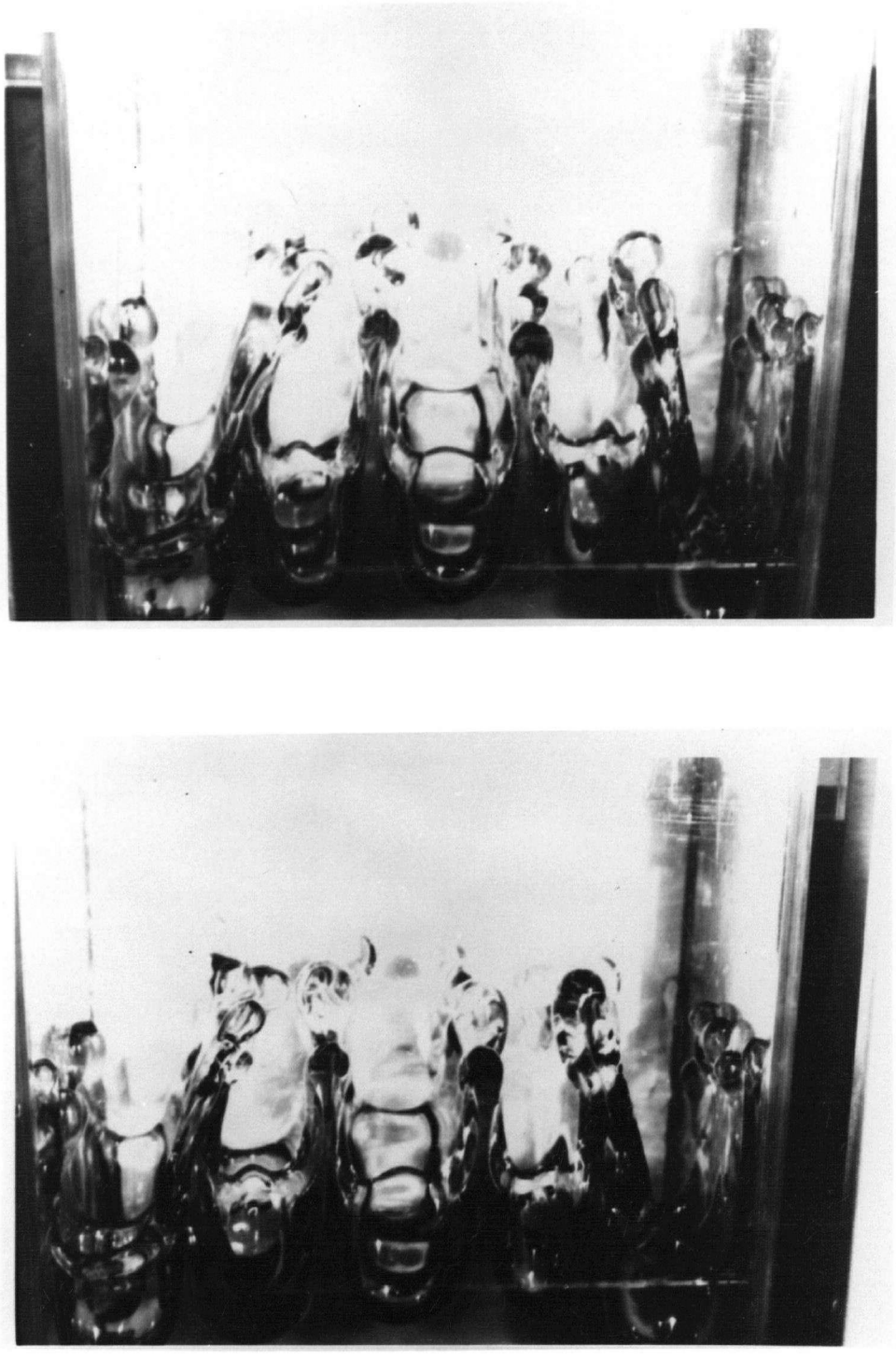

Figure 28. The eighth harmonic instability with the initial phase $\Phi=\pi$.

In order to suppress the mode across the narrowest dimension of the water surface another tank was constructed such that its width was less than the cut-off wavelength for this mode:

$$\lambda_c = 2\pi (T/g\rho)^{\frac{1}{2}}$$

For water the surface tension T is 75 dynes/cm and the density ρ is 1 g/cm^3 so that for a typical acceleration of 1.5 g the cut-off wavelength is about 14 mm.

Because of the large damping due to the reduced cross sectional area of the narrow tank, the amplitudes of the electrically driven waves are much less than the 1.5 mm obtained previously in the wider tank. Nevertheless, the final amplitude of the instability was observed to be about the same as in the wide tank about 9 cm in this case. The photographs of the q=4 mode instability in the narrow tank (Figure 29), show that the resulting motion is much more two dimensional.

However, due to the smaller width, the meniscus forms a considerable part of the initial unaccelerated surface. When the tank is accelerated this film is seen to climb up the walls of the tank. In the wide (10.5 cm) tank, the film's amplitude is about half that of the instability. In the narrow tank, the film now reaches the same height as the spikes.The film appears to be of uniform thickness throughout except near its edge

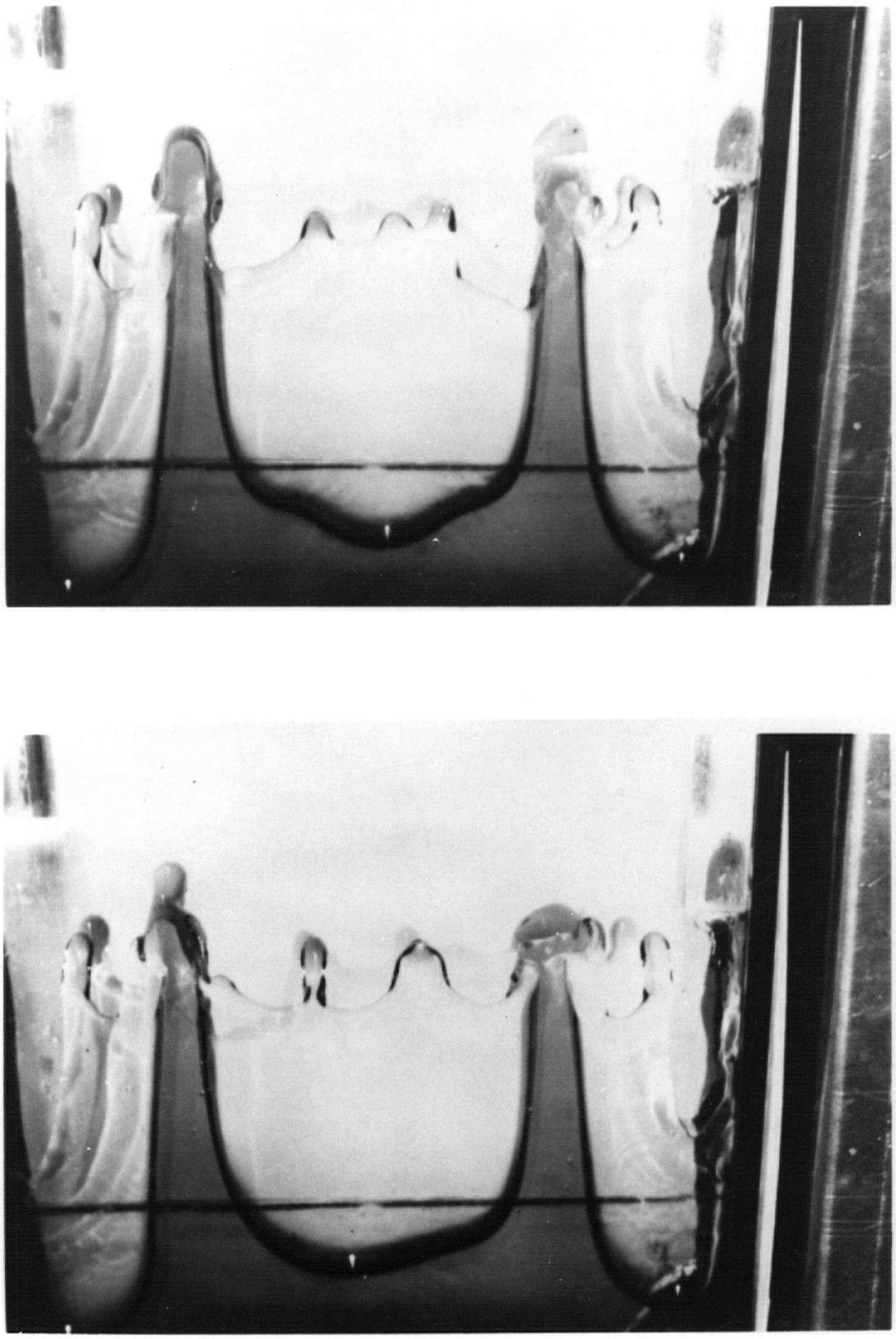

Figure 29. The fourth harmonic instability in the narrow tank of 1.5cm. Here the motion appears to be two dimensional.

where it bulges. To estimate how much fluid is in the film, the weights of various regions of the photograph were compared (Figure 29). It was found that the weights of the spikes above the intial level and the troughs (or bubbles) below it balanced to an accuracy of 10%.

E. Electrical Measurements using the Narrow Tank

Although the 4th harmonic instability in the narrow tank appears to be two dimensional, the capacitance bridge measurements indicate the contrary. By setting the bridge capacitance to a value lower than that of the unaccelerated tank, the resulting signals from the bridge are observed to go through zero as shown before in figure 14c). This indicates once again that the capacitance and hence the mean level decrease with time. As in the case of other modes, the signal growths appear to change linearly with time. Runs were done at various accelerations up to 3.0 g, yet there appears to be no difference between the runs which had the initial surface excited and those which had the initial surface unperturbed (Figure 30).

The saturation of the signal growths is a characteristic feature common to all runs done by using the capacitance bridge. The level at which the saturation

a)

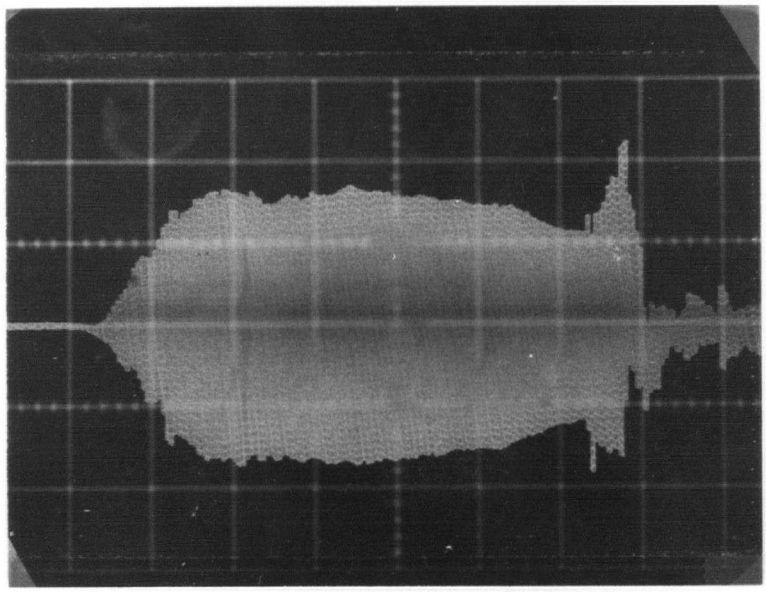

b)

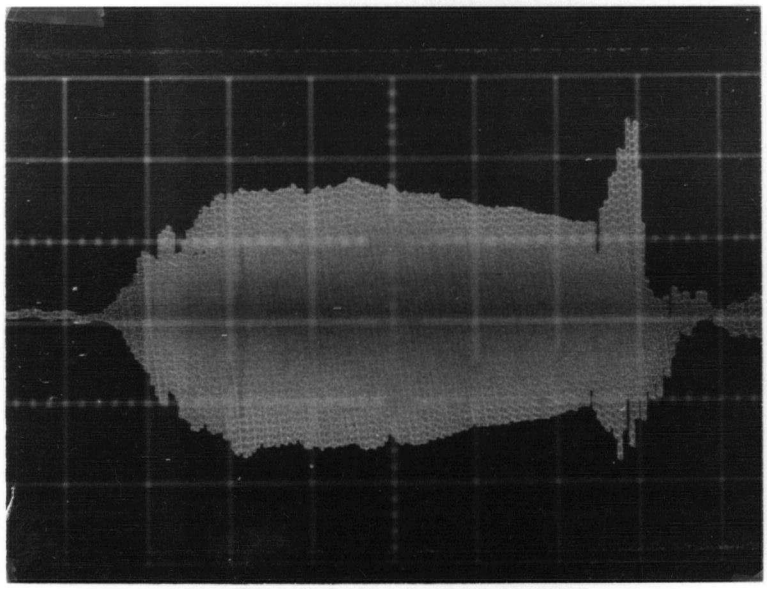

Figure 30. Capacitance bridge signals versus time for the fourth harmonic instability in the narrow tank. Gain is 0.2v/div, time base is 20 msec/div.
a) unperturbed surface
b) excited wave surface
Acceleration for both runs was 1.5 g's.

of the growth occurs indicates that there is a change in capacitance corresponding to a change in depth of 5-6 cm. This is not an effect due to the bridge characterictics as the bridge calibration was verified to be linear up to a depth change of 11 cm prior to obtaining the oscillographs in Figure 30. Since it is established that the capacitance decreases as a function of time, the results imply that the there is an air film between the water and the wall such that the contact area is diminished to a depth of several centimeters.

The decrease in the mean level was checked again using the resistance method. Two plain copper plates were placed on the inner sides of the larger walls of the narrow tank. Upon accelerating the tank at 2.0 g virtual acceleration, a rise in the voltage drop across the tank was observed (Figure 31). In this case, the oscillograph represents the d.c. signal across the tank and hence shows the bias voltage drop of about 5 volts. Since there is a positive increase in the bias voltage, this confirms the capacitance bridge test that the mean level does decrease with time.

To verify that voltage across the tank does indeed increase as the water level falls, the tank was drained with a siphon and the output voltage was displayed on a storage oscilloscope. In Figure 32 a), the initial water level was 22 cm measured from the

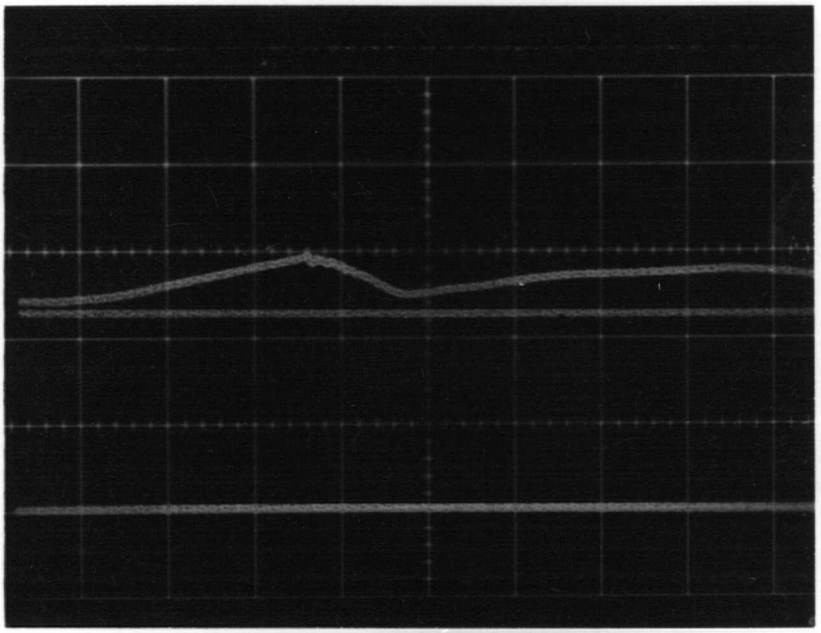

Figure 31. Check of change of mean level using the resistance method. First line in the oscillograph is the d.c. voltage across the tank during a run at 2.0 g's acceleration. Third line is the ground reference. Gain is 2v/div and the time base is 50 msec/div.

a)

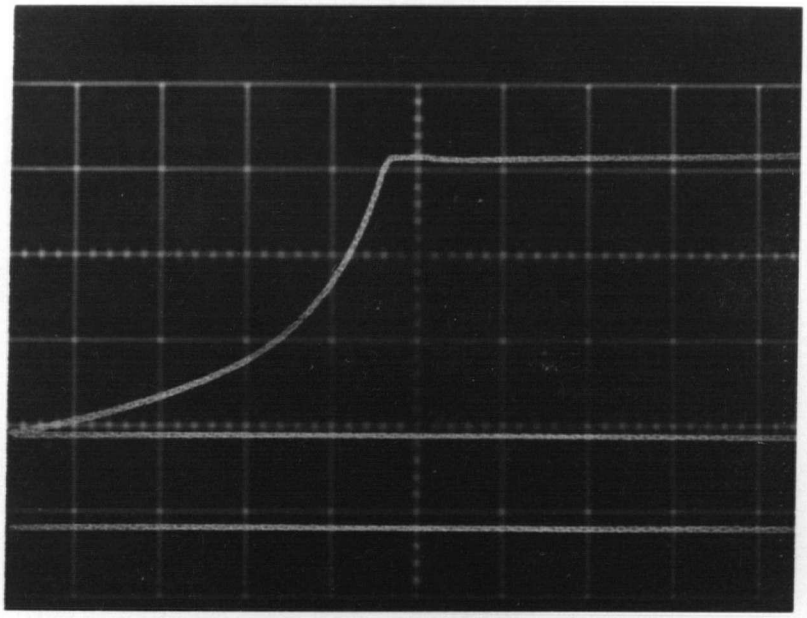

b)

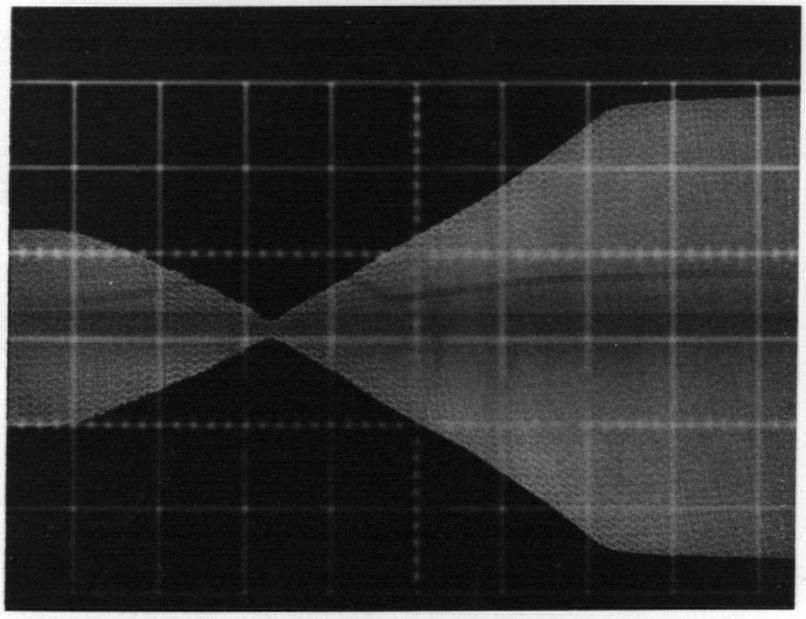

Figure 32. Check of validity of growth direction tests.
a) Resistance method. Voltage across the tank as water is drained through a siphon. Gain 2v/div, time 5sec/div.
b) Capacitance bridge. The water approaches the balance level and recedes beyond it, thus the "pinching" of the envelope occurs at the balance level. Gain 0.1v/div, time 5sec/div.

bottom corresponding to a bias voltage of about 2 volts and was drained to a level of 3 cm resulting in a voltage drop of about 6 volts.

The same sort of check was performed using the capacitance bridge shown in Figure 32 b). Here, the water level was initially 1 cm above the "balance" or null signal level and it was allowed to decrease to 3 cm below this level. The oscillographs in figure 31 verify that when the mean water level decreases linearly, the voltage in the resistance method increases in a hyperbolic fashion and the capacitance bridge output decreases as the water level approaches the balance level.

Therefore, although photographs of the 4th harmonic instability show an apparently two dimensional waveform, the electrical measurements described would seem to indicate that there is a decrease in the mean level as the tank is accelerated and thus the feasibility of doing a Fourier analysis using the given techniques is nullified.

F. Test for the Air Film

Since the capacitance bridge signals (Figure 30) suggest that an air film must get between the water and the walls of the water tank, a test for the presence of

this film was devised. The basic principle was to use a helium-neon laser beam to reflect off the Plexiglas-air or water-air interface. Simple calculations using Snell's law show that the critical angle for total internal reflection is the same for the two interfaces and is about 42^{o}.

To obtain the proper geometry for total internal reflection a Plexiglas prism 20 cm long and 2 cm wide was made and glued onto the face of the narrow tank (Figure 33). A lens was placed in front of the laser to spread the beam to a diameter of about 1.5 cm. The beam was incident onto the 50^{o} face of the prism (Figure 33), and its angle of incidence adjusted so that the total internal reflection occurred whenever there was air on the other side of the Plexiglas wall containing the prism. The reflected light was detected by a phototransistor whose output was monitored on a storage oscilloscope. To detect the air film that exist below the initial water level, the prism above this level was masked off.

The results are shown in Figure 34. In 34 a), the pulses are solely due to stray reflections from the prism and tank as it was accelerated past the phototransistor. In 34 b), a sharp pulse due to internal reflection occurs. However, the duration of this pulse (about 0.004 sec) appears to be much shorter than expected

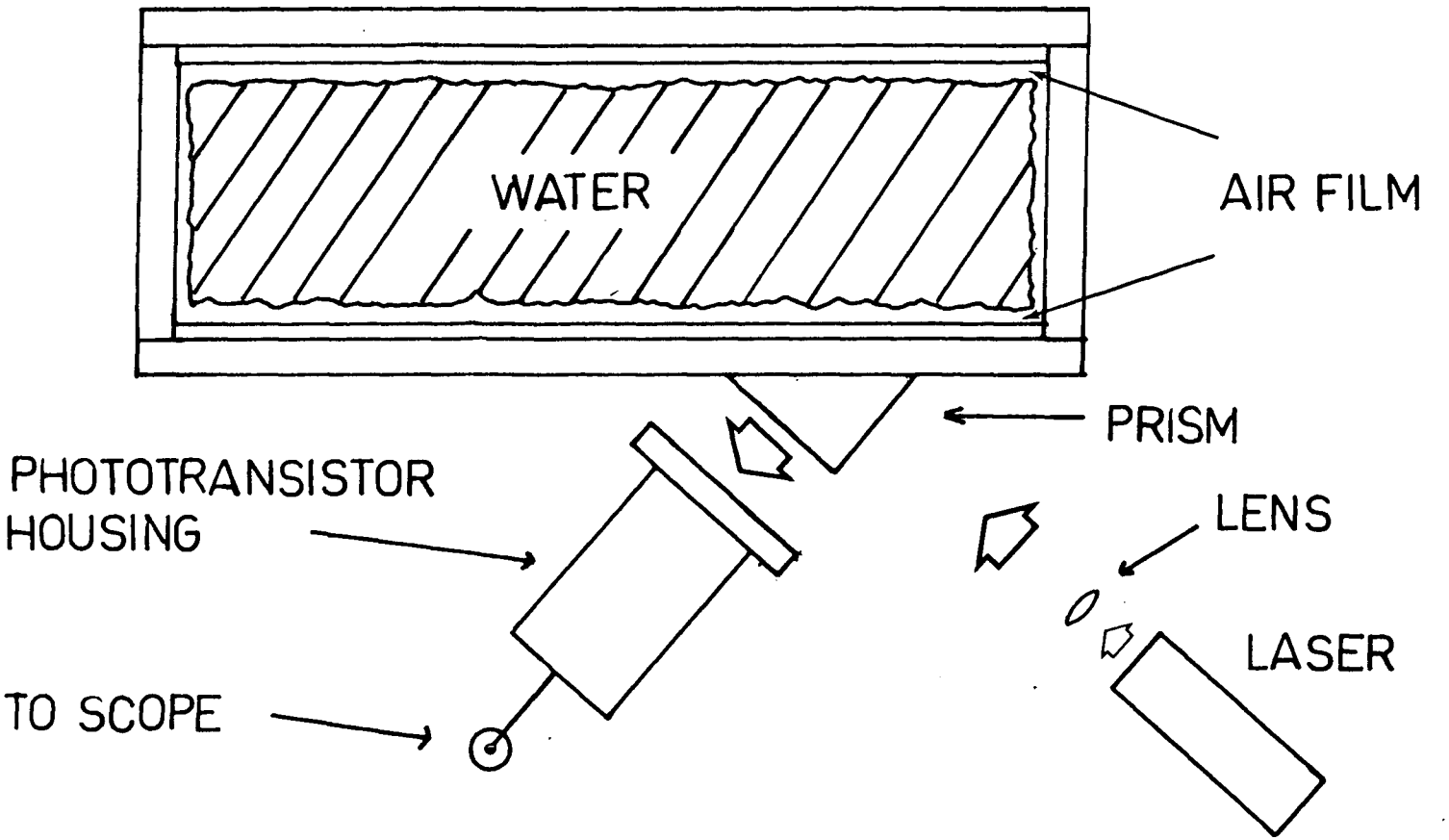

Figure 33. Schematic of the test for the presence of an air film using total internal reflection from a Plexiglas-air interface.

a)

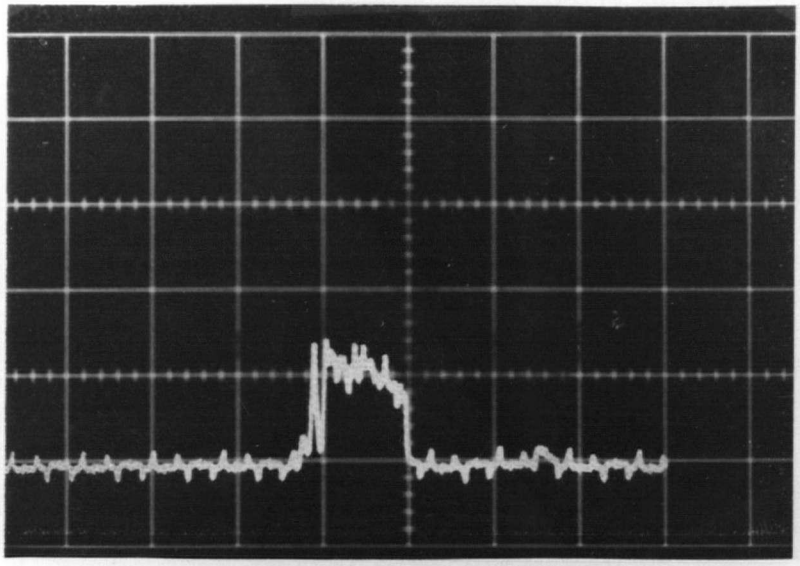

b)

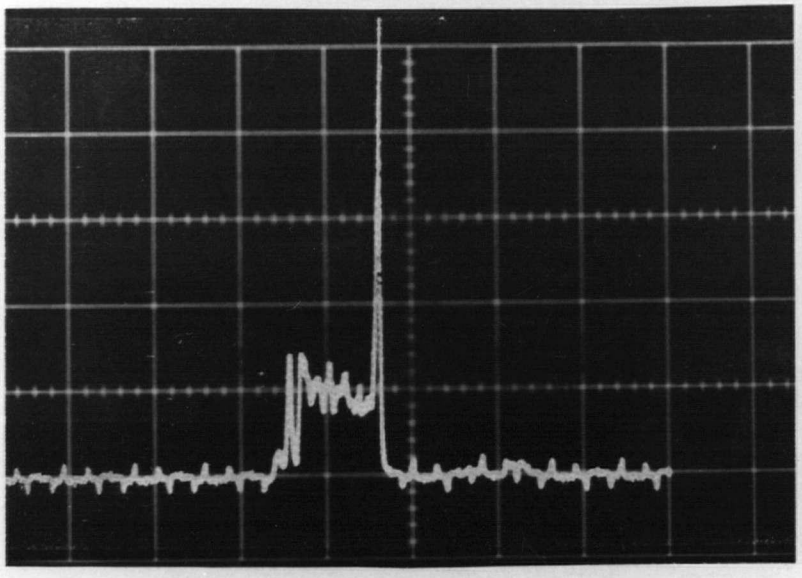

Figure 34. Test for the presence of an air film. Output from the phototransistor.

a) Pulses due to stray reflection off the tank accelerated at 2.0g's.The water level was 3cm above the masked portion of the Plexiglas prism.

b) Pulses due to stray reflections plus a sharp large peak due to internal reflections due to the presence of an air film.The water level was 3mm above the masked half of the prism.

Gain for both oscillographs is 2mV/div,time 20msec/div.

if an air film penetrates a distance of several centimeters below the initial water level.

Another indication that the air film amplitude is considerably less than expected is the fact that the sharp pulse disappeared when the initial water level was set at 7 mm above the masked off porion of the prism; the internal relection reoccurred when the initial level was lowered to 5 mm. This shows that the amplitude of the air film is not greater than 7 mm. The low figure for the amplitude of the air film is now more consistent with the result obtained using the resistance technique (Figure 31). There, the change in d.c. voltage corresponds to a change in mean level of less than 2 cm, considerably less than the 6 or 7 centimeters suggested by the capacitance bridge runs.

The resistance and internal reflection results imply that there is some other effect that is causing the large signals from the impedance bridge. Since the water under acceleration is under considerable tension, it was suspected that the water's adhesion to the dielectric sheet causes the latter to be pulled away from the capacitor plate creating an air space between the dielectric polyethylene sheet and the capacitor plate. This process increases the thickness of the effective dielectric resulting in a decreased capacitance.

The problem of the air film was finally resolved

when a new capacitor plate was fashioned from a printed circuit board sheet which now provided both the dielectric layer and the conducting plate. The plated side of the board formed the outside wall of the tank. Due to the comparative thickness of the fiber board dielectric, the tank's capacitance when half-filled with water was now 885 pF instead of the 2,200 pF obtained with the polyethylene sheet dielectric.

Nonetheless, upon excess acceleration of 1.5 g the capacitance bridge output now showed a strikingly smooth growth envelope that was not linear (Figure 35). Similar tests to those described in Chapter 3 part A, show that the capacitance increases with time, a result consistent with the movement of water layers up the walls of the accelerated tank.

G. Climbing Films

Plots of the square root of the change in capacitance versus time yielded straight lines (Figure 36). This indicates that the edge of the water film moves up the tank wall at a constant acceleration. A similar observation was made by Emmons et al using photographic observations.

Several runs were made varying the virtual acceleration from 1.7 to 4.7 g. Plots of the square root

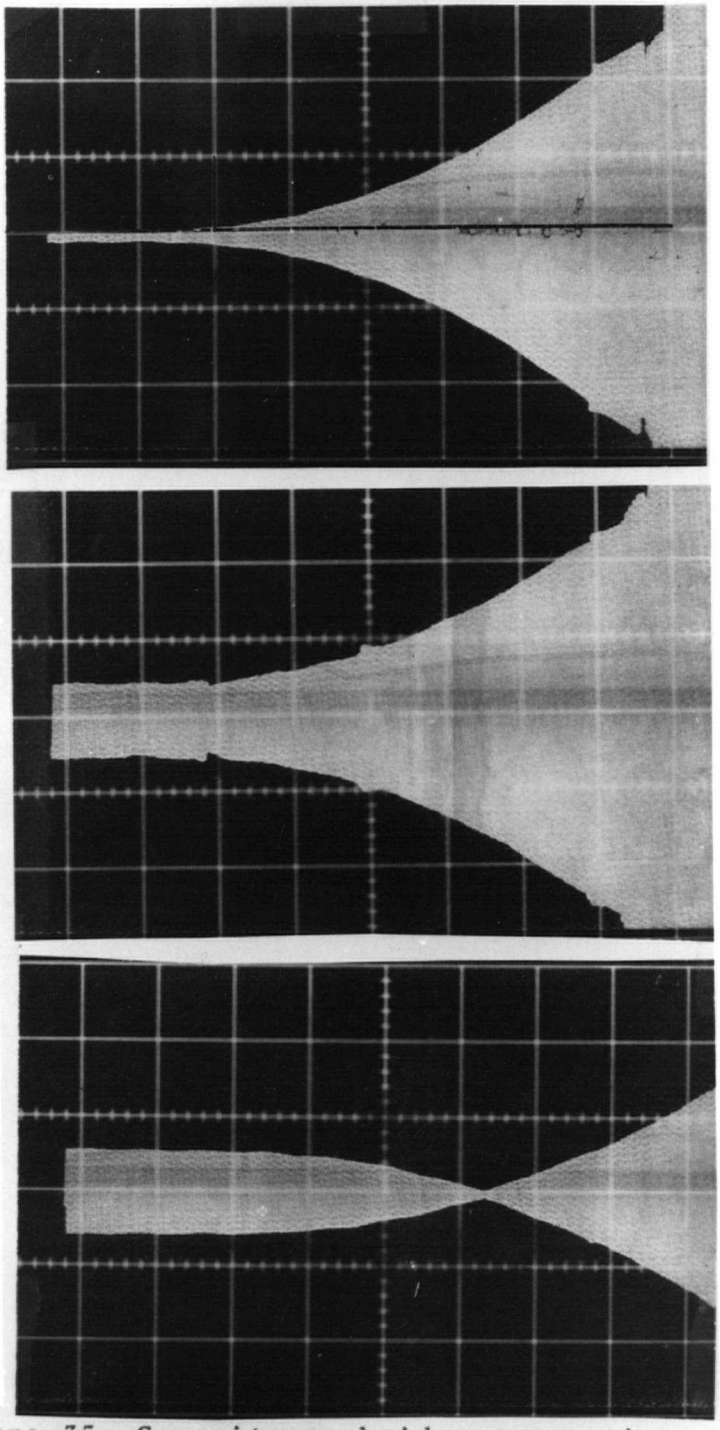

Figure 35. Capacitance bridge runs using a printed circuit board as the dielectric and capacitor plate.

a) A run with the bridge initially balanced at the water level capacitance.
b) Here the bridge was balanced below the initial water level.
c) In this run the bridge was balanced above the initial level capacitance.

Gain for all shots is 0.2v/div, time is 20msec/div.

of the amplitude s of the film versus the time t indicate that the acceleration of the film is less than the virtual acceleration (Figure 36). The ratio of the film acceleration to the virtual acceleration varied from about 0.3 at 1.7 g to 0.6 at 4.7 g.

When the slopes of the $\sqrt{s}$ versus t graphs were plotted against the applied virtual accelerations straight lines passing through the origin were obtained (Figure 38). Runs were made using an aqueous soap solution as well as a 40% sugar solution to determine if surface tension or viscosity has an effect. In all cases the results are about the same as that for ordinary water and are presented in table V.

TABLE V : CLIMBING FILMS RESULTS

FLUID	SLOPE ($cm^{-\frac{1}{2}}sec$)	INTERCEPT ($cm^{\frac{1}{2}}sec^{-1}$)	CORRELATION COEFFICIENT
Water (viscosity 1 cP, surface tension 75 dynes cm^{-1})	0.00792	1.526	0.9929
Soap solution (viscosity 1 cP, surface tension ~ 35 dynes cm^{-1})	0.00820	2.398	0.9866
40% Sugar solution (viscosity 5.164 cP)	0.00740	0.569	0.9976

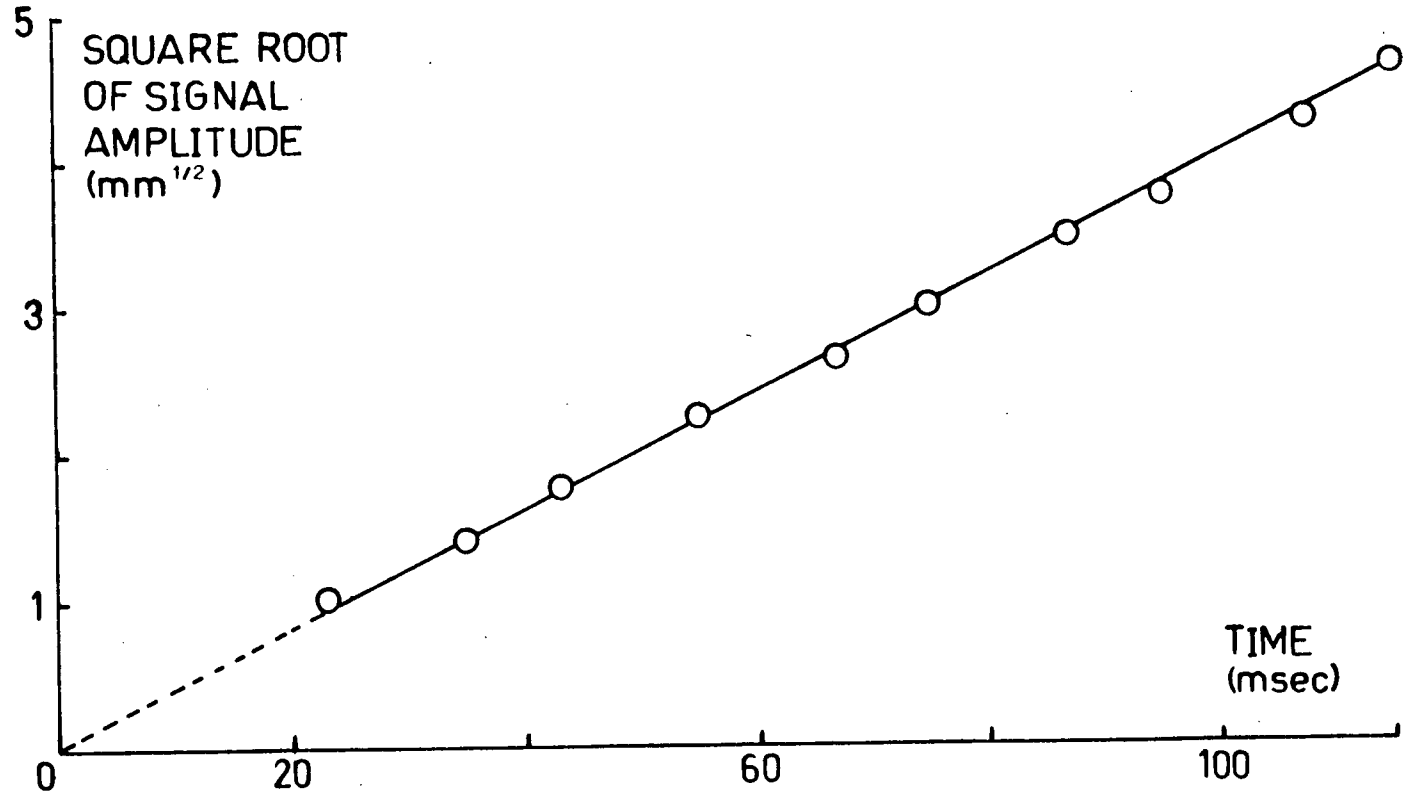

Figure 36. The climbing film. The square root of the signal amplitude of figure 35 a) is plotted as a function of time.

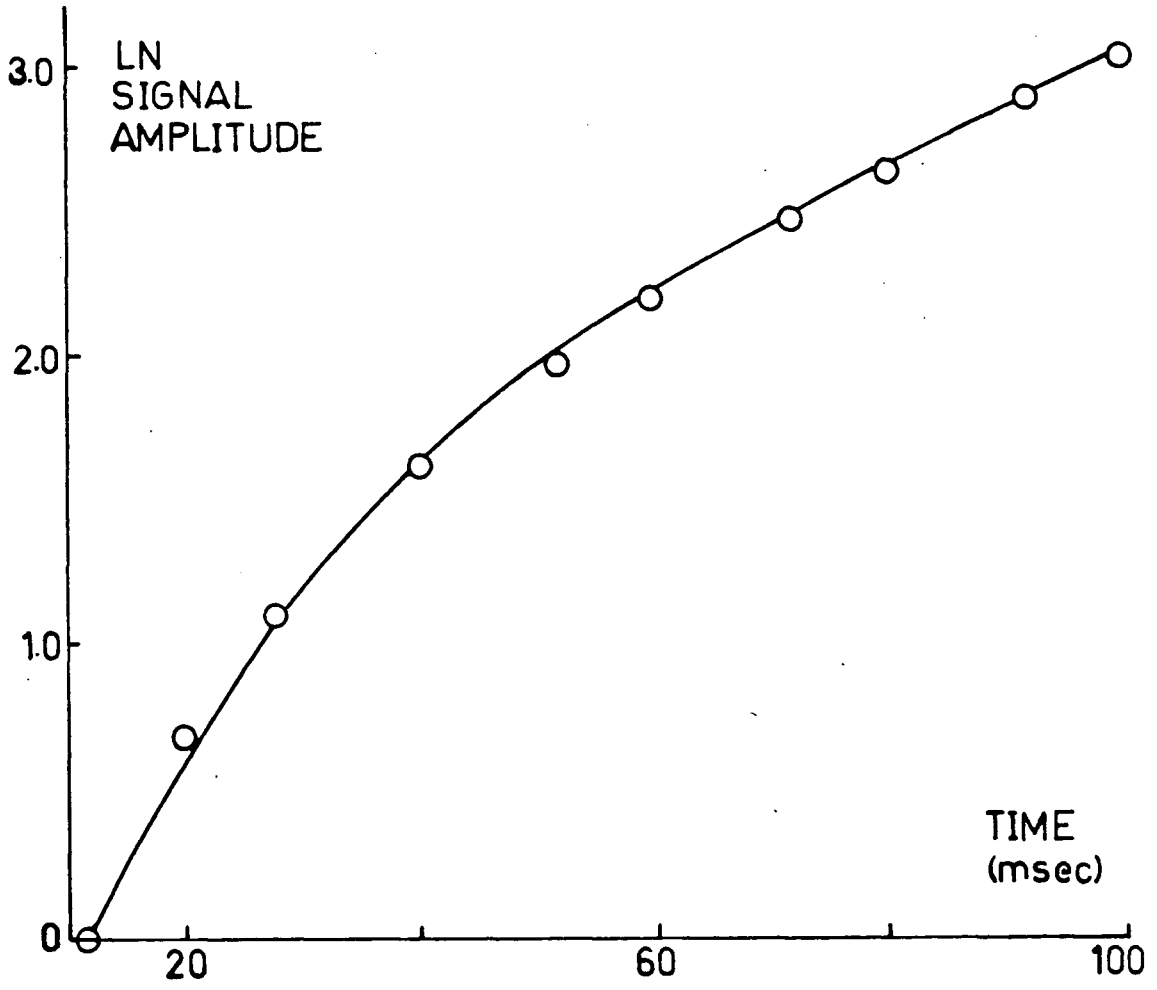

Figure 37. The climbing film. The logarithm of the signal amplitude of figure 35 a) is plotted against the time. The graph above indicates the the signal growth is not due to an instability.

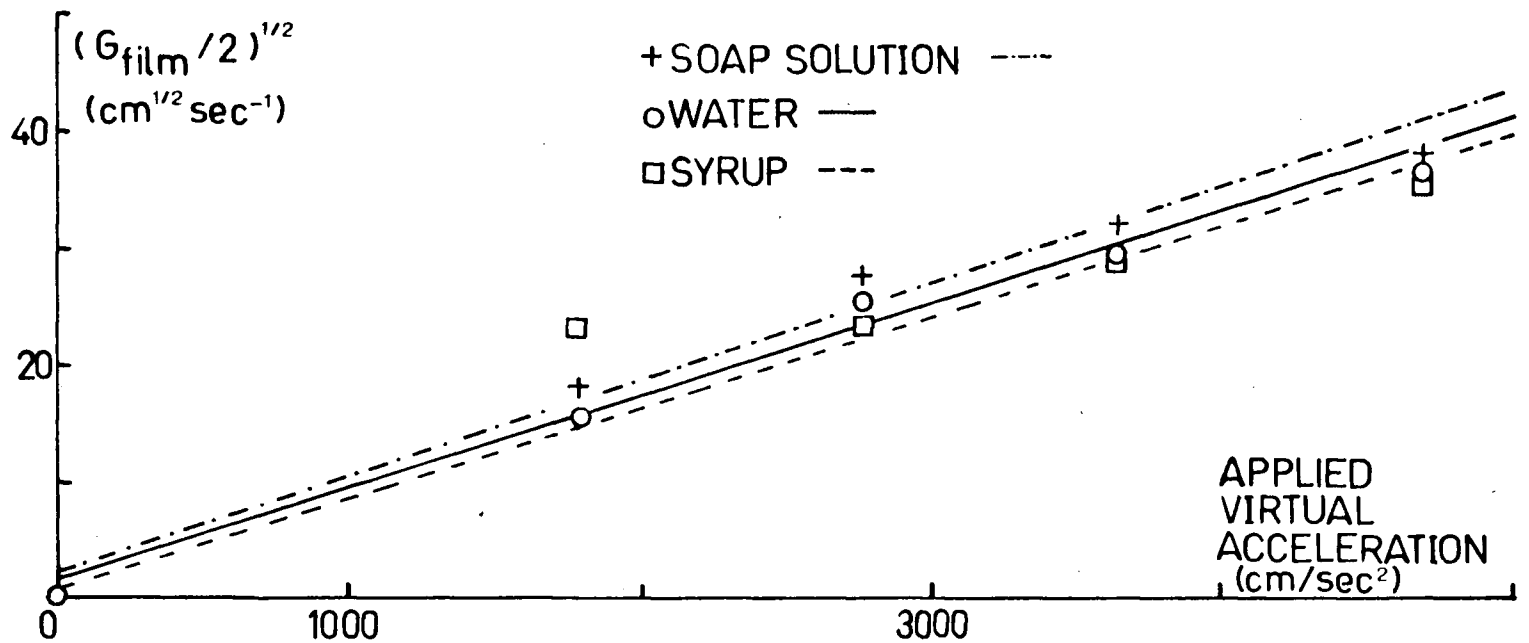

Figure 38. The climbing films results. The square root of the acceleration of the film is plotted versus the applied virtual acceleration. The results for different fluids are shown.

Thus, from table V, the scaling law for the behaviour of the climbing films with applied acceleration is

$$g_{film} = 1.25 \times 10^{-4} cm^{-1} sec^2 (g_{virtual})^2$$

Using the printed circuit board as the dielectric and capacitor plate shows conclusively that the previous capacitance bridge signals were caused by the water pulling the dielectric sheet away from the wall. Since the tension on the water is proportional to the acceleration, the amount of air that gets in between the dielectric sheet and the capacitor plate can be expected to be proportional to the applied acceleration as well. Indeed, the rate of decrease of capacitance was seen to be proportional the the virtual acceleration. This also explains why the earlier capacitance bridge signals are seen to saturate so quickly. The dielectric sheet simply becomes pulled away from the wall to its limit and stays there.

However, Fourier analysis using the capacitance bridge still cannot be done because of the presence of climbing water films. This is particularly the case in the narrow tank where the films are quite predominant and actually have the same amplitude as the instability. In the wide tank, the films are seen to lag somewhat behind the instability and as Figure 23 shows, a thin film can be seen to reach about half the amplitude of

the spike. In this case, the films are much thicker in the rounded bubbles, and thus there may be some possibility of distinguishing between capacitance bridge signals for runs with excited and unexcited initial surfaces.

The problem of the climbing water films can be eliminated altogether if an optical Fourier analyzer technique were to be used. Since the absorption of light varies as the exponential of the thickness of the absorbing medium, the films of water that appear along with the instability should then not be noticeable in darkened water. This technique would consist of replacing the analyzing capacitor plate with a photographic negative of the same. Parallel light is incident on one face of the narrow tank and a photodetector is on the other side of the Fourier plate negative. The photodetector should be saturable such that its output is proportional to the amount of area exposed to light and is largely independent of the light intensity. The signal output from the photodetector should then give the development of the instability. Details of the technique are discussed in the Appendix.

CHAPTER IV

CONCLUSION

In the course of my experiments, I have developed an apparatus which produces large amplitude reproducible Rayleigh-Taylor instabilities from a pure sinusoidal standing wave. Timing circuitry was developed such that the phase of the standing wave and thus the shape of the resulting instability could be set exactly. This allows the measurement of the amplitude variation of the instabilities as a function of time to be compared directly with theory. This is in contrast to all other previous experiments where the initial perturbation, phase and resulting instability were largely left to chance.

I developed three novel electrical measurement techniques for the detection of standing water waves. The simplest is the resistance method where the voltage across the tank is measured using Fourier analyzing plates as the electrical contacts.Another method uses a simple frequency to voltage converter to measure the capacitance of the water tank. The third method uses solar cells to measure the light transmitted through a transparency of the Fourier analyzing plate. All these methods have sufficient sensitivity that small standing waves of amplitudes of about 1 mm or less are readily detected.

The electrical measurements I used to observe Rayleigh-Taylor instabilities revealed features of the instability that were not considered prior to the course of the experiments. Namely, the electrical measurements indicated a convex bulging of the water surface across the width of the tank. This results in a decrease in the mean level of contact of the water with the walls.

Photographs of the instabilities confirm this bulging of the water surface, as well as the presence of climbing water films that keep pace with the instability. These water films unfortunately indicate that a capactative Fourier analysis will not work as the method is unable to distinguish the water films from the instability. However, the capacitative transducer can now be easily used to do studies of the climbing water films as a function of the applied excess acceleration. Observations of the capacitance bridge signals vs. time indicate that the edge of the water film moves at a constant acceleration which is a fraction of the downward acceleration of the water tank.

Plots of the square root of the film acceleration versus the applied acceleration yielded straight lines passing through the origin. The scaling law for this behaviour has been determined to be:

$$g_{film} = 1.25 \times 10^{-4} sec^2 cm^{-1} (g_{virtual})^2$$

and was found to be independent of the surface tension and the viscosity of the fluid.

Attempts to eliminate the convex bulging of the fluid by decreasing the width of the tank to 1.5 cm (less than the length of the critical wavelength at modest accelerations) have been successful. Photographs of the instability show that it is much more two dimensional than the same instability in a tank that is several centimeters wide. The same photographs also indicate that the climbing water films are of uniform thickness and are relatively transparent compared to the bulk of the dyed water in the rest of the tank. This result suggests that Fourier analysis is feasible if an optical technique is used instead. This technique works on the same principles as the capacitative and resistive methods, the major difference being that since absortion of light is the major factor, the comparatively thin water films should not now be detectable.

BIBLIOGRAPHY

Bellmann R., Pennington R.H., Quart. J. Appl. Math. 12, 151 (1954)

Cole R.L., Tankin R.S., Phys. Fluids 16, 1810 (1972)

Curzon F.L., Langille B.L., Can. J. Phys. 50, 73 (1972)

Emmons H.W., Chang C.T., and Watson B.C., J. Fluid Mech. 1, 177 (1960)

Langille B.L., M.Sc. Thesis, University of British Columbia (1970)

Lewis D.J., Proc. Roy. Soc. A 202, 81 (1950)

Popil R., Curzon F.L., Rev. Sci. Ins. 50. 70 (1979)

Ratafia M., Phys. Fluids 16, 1207 (1973)

Stoker J.J., Water Waves; The Mathematical Theory with Applications, Interscience Publishers (1957)

Taylor G.I., Proc. Roy. Soc. A 201, 192 (1950)

APPENDIX A : Details of the Waveform Generator

To produce pure mode standing waves on the water surface, an electric field of the form

$$V = V_o (\{1 - \cos(\omega t)\}/2)^{\frac{1}{2}}$$

is used. Initially, a digital waveform generator is used to produce a 5 volt peak to peak signal which is then amplified by an inverting amplifier with a gain of 1000. The schematic diagrams of the generator are presented along with an explanation of its operation.

There are three main sections to the generator (Figure 39 a)). An oscillator provides pulses which advance the address on an up/down counter that scans the 16 words of the two 4-bit memories (RAM). The output of each word from the memory is converted to an analog signal which is consequently amplified and used to excite standing waves.

Square wave pulses from a set of frequency dividers are entered into the circuit through the input labelled the "CLOCK INPUT". The clock pulses enter the up/down counter through the OR gates of 3003. To count upwards from 0 to 15, the up/down counter requires the C_{up} input to be pulsed and the C_{down} input to be high. This condition is provided by the Q and $\overline{Q}$ outputs of the JK flip-flop 3062 which are set high

a)

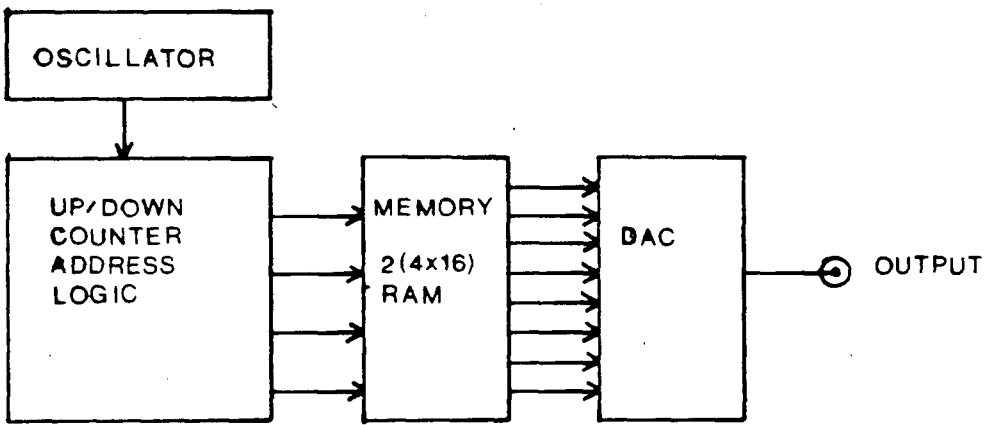

b)

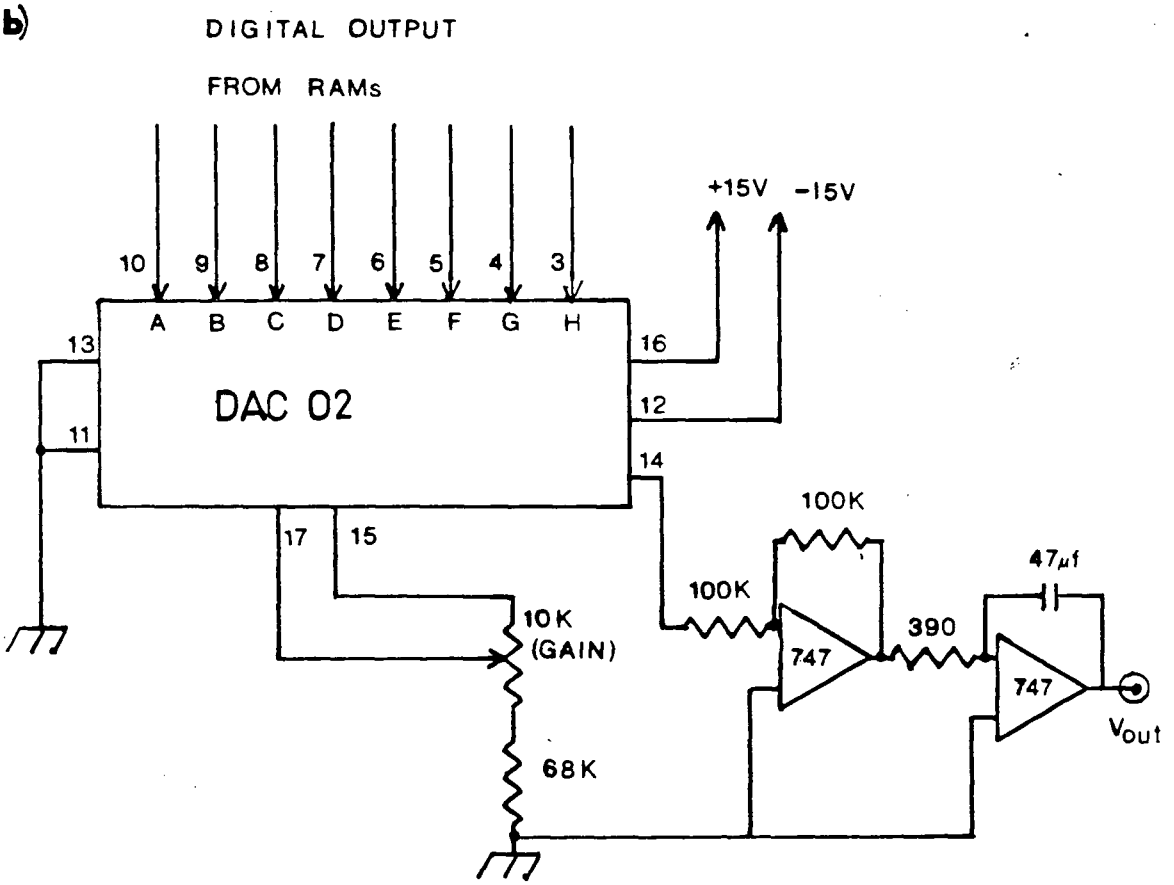

Figure 39. Schematic of the digital waveform generator.
a) Block diagram
b) The digital to analog converter and output stage.

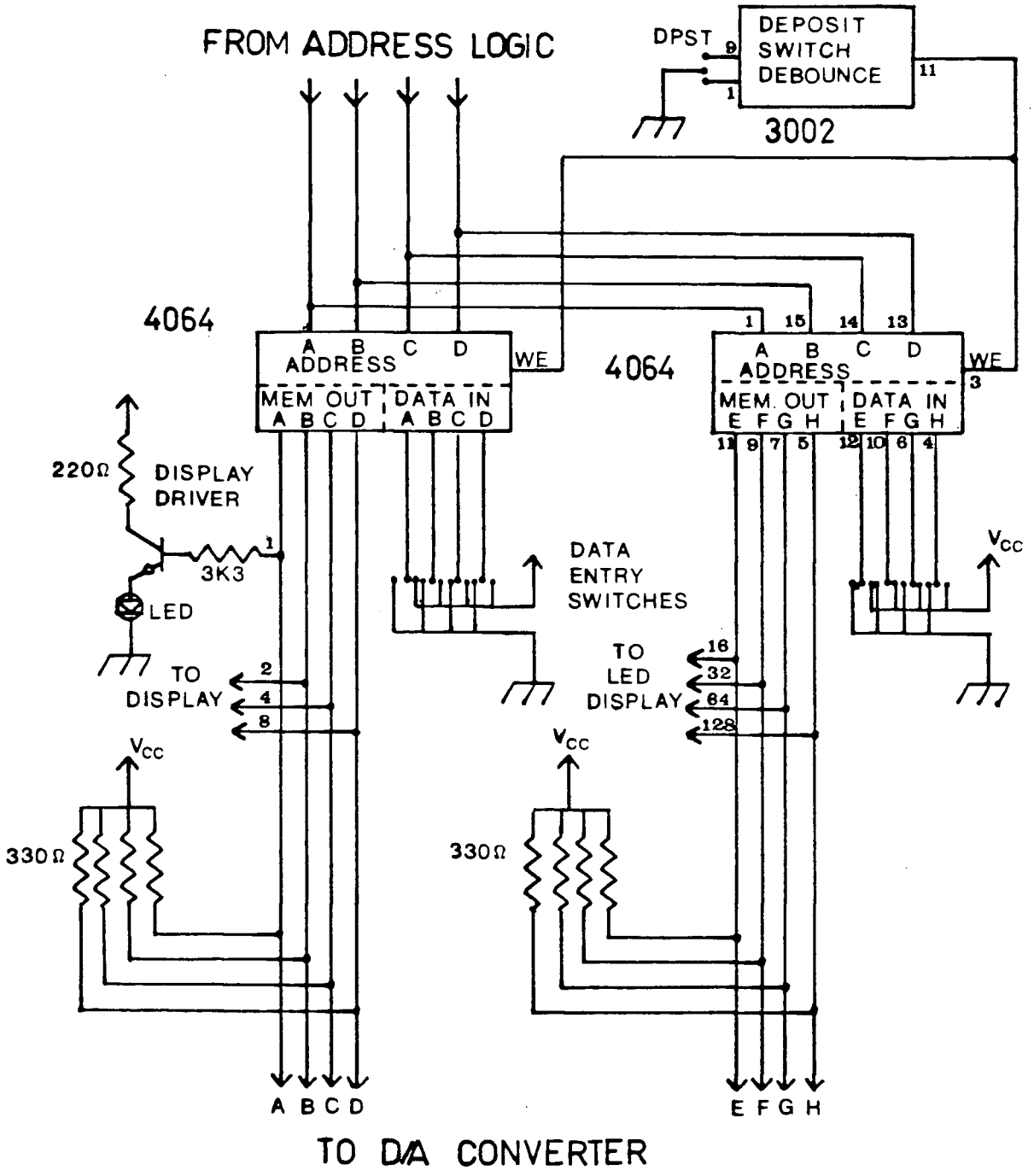

Figure 40. The waveform generator: memory and display section.

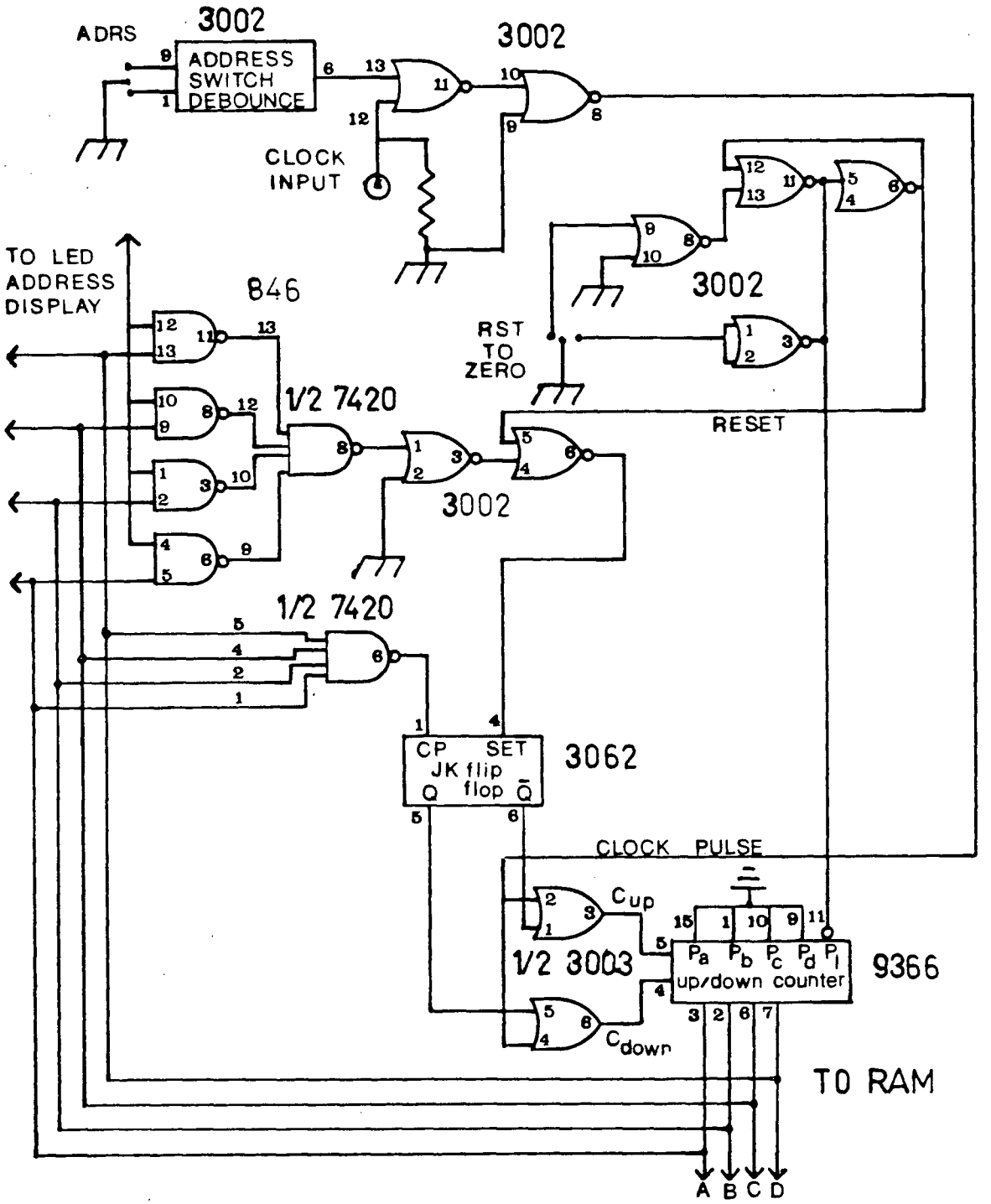

Figure 41. Detail of the up/down counter address logic.

and low respectively for the count upwards. When the output of the up/down counter is 0000, the asynchronous $\overline{SET}$ input of the JK flip-flop receives a LO input that sets the flip-flop for the count upwards. When the count upward terminates at 1111, the flip-flop is triggered by the LO signal applied to the clock pulse input CP, which now reverses its state to Q = 0 and $\overline{Q}$ = 1. The clock pulses will now make the counter count backwards to 0000 and the above operations automatically repeats itself.

Thus, the up/down counter produces a 4-bit word which is incremented at every clock pulse. This address word reaches the two RAM memories which then output a corresponding 8 bit word stored at that particular address. This 8 bit word is finally converted to an analog signal by the digital to analog converter (I.C. DAC 02), so that any waveform entered into the memory will be periodically generated.

To enter a periodic function into the waveform generator's memory, the clock oscillator is disconnected and the address is reset to zero by a push button reset switch that simultaneously sets the flip-flop to the count-up position and sets the flip-flop to the count-up position and sets the up/down counter to 0000 by means of a low pulse sent to the P_L input. One half of the desired function is approximated by 16 steps in digital

form and are entered manually on the data entry switches. To deposit a word into the memory by the switches, the write enable (WE) input is activated by the deposit switch and the word is entered into the memory at the address location displayed. The address is then incremented manually to the next sequential address and the procedure is repeated until all 16 addresses have been filled.

The program for the program used to excite standing waves is included in table VI.

TABLE VI : DIGITAL PROGRAM FOR WAVE GENERATOR

ADDRESS	WORD (ENTERED ON SWITCHES)
0 0 0 0	1 0 0 0 1 1 0 1
0 0 0 1	1 0 0 0 1 1 0 0
0 0 1 0	1 0 0 0 1 0 0 1
0 0 1 1	1 0 0 0 0 1 1 0
0 1 0 0	1 0 0 0 0 0 0 1
0 1 0 1	0 1 1 1 1 0 1 0
0 1 1 0	0 1 1 1 0 0 1 0
0 1 1 1	0 1 1 0 1 0 0 1
1 0 0 0	0 1 1 0 0 0 0 1
1 0 0 1	0 1 0 1 0 0 0 1
1 0 1 0	0 1 0 0 1 0 1 1
1 0 1 1	0 0 1 1 1 1 1 1
1 1 0 0	0 0 1 1 0 1 0 0
1 1 0 1	0 0 1 0 1 0 1 0
1 1 1 0	0 0 1 0 0 0 0 1
1 1 1 1	0 0 0 1 1 1 1 0

APPENDIX B : OPTICAL FOURIER ANALYSIS

The experimental set-up for the Fourier analysis by an optical technique is shown in Figure 41. The suggested configuration requires very little construction of any apparatus and is designed to withstand accelerations of several g. A panel of solar cells are rigorously mounted to the outside face of the side of the tank containing a photographic negative of the Fourier analyzing plate. Because of their voltage-current characteristics, the output terminals of the solar cells must be kept at ground voltage in order to achieve linearity between light intensity and the current output. To this end, the positive terminal of the solar cells is connected to a virtual ground, current to voltage converter as is shown in the figure. To observe changes in the output voltage due to surface waves or instabilities, the d.c. bias voltage can be eliminated by using a differential amplifier anda variable d.c. voltage source.

To obtain uniform parallel incident light, the easiest solution is to have a point light source such as a d.c. arc, placed a suitable distance away from the front face of the water tank. Thus, there is no need of mounting optical components onto the tank.

About 5cc of water soluble ink mixed into two liters of water adequately darkens the water. The resulting

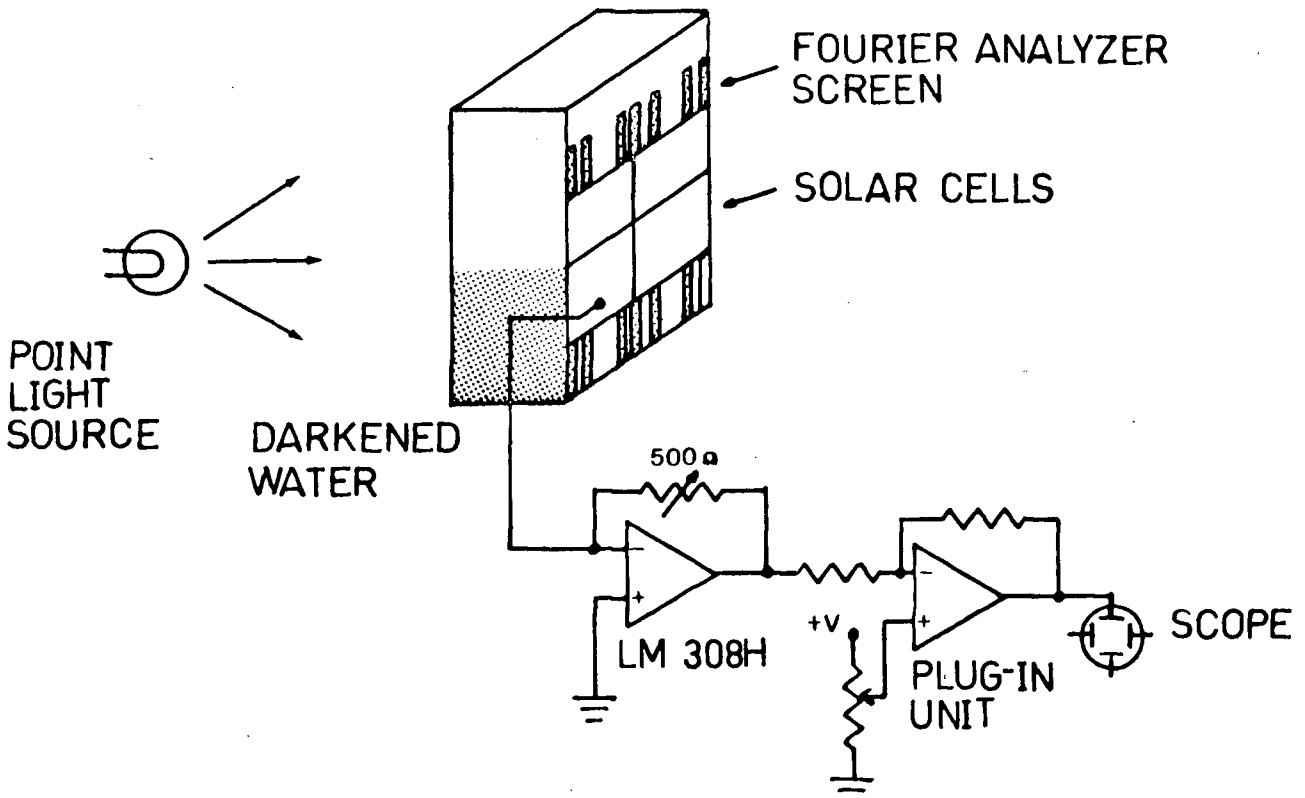

Figure 42. Experimental set-up for the optical Fourier analysis of R-T instabilities. The figure also shows the current to voltage converter.

films of water which appear at the sides of the tank upon its acceleration should not now interfere with the detection of the instability.

The current to voltage converter has been made and tested using the solar cells. The 50 Ω resistor is adjusted to a value such that the saturation of the op amp is avoided under the experimental conditions. The tentative tests show that the arrangement is linear with respect to the area exposed to light. For the 1.5 mm 4th harmonic standing waves a sinusoidal signal of amplitude 60 v_{p-p} was obtained indicating that this method of wave detection is as sensitive as the I.C. circuit described in chapter II part E.

On the basis of the above observations, the Fourier analyzing technique using the solar cells appears to be quite promising on the whole.